

JURASSIC SEDIMENTARY EVOLUTION OF A CARBONATE PLATFORM INTO A DEEP-WATER BASIN, MT. MANGART (SLOVENIAN-ITALIAN BORDER)

ANDREJ ŠMUC¹ & ŠPELA GORIČAN¹

Received: July 30, 2003; accepted: July 27, 2004

Key words: Jurassic, platform drowning, eustasy, subsidence history, Radiolaria, Southern Alps, Slovenian Basin, Belluno Basin.

Abstract. A complete Jurassic succession, recording the evolution from platform margin to a deep-water basin, is exposed at Mt. Mangart in the Julian Alps. The succession is a part of the Julian Nappe, where the Southern Alps overlap with the Dinarides. In the Jurassic, the area comprised part of the south Tethyan passive continental margin. The section was studied sedimentologically in detail and dated with radiolarians. It is divided into five lithostratigraphic units: Unit 1: Lower Jurassic shallow-water peloidal and oncoidal limestones; Unit 2: Pliensbachian distal shelf limestones rich in juvenile ammonites and sponge spicules topped by an Fe-Mn hardground; Unit 3: lower to possibly middle Toarcian sequence of black shales with interbedded siliceous limestone; Unit 4: upper Bajocian/Bathonian to lower Tithonian cherts, cherty limestones, and carbonate gravity-flow deposits; Unit 5: upper Tithonian red nodular cherty limestones with abundant calpionellids and aptychi. A stratigraphic gap, comprising the late Toarcian to early Bajocian, separates Unit 4 from Unit 3.

In general, the succession correlates well with known Tethyan transgressive/regressive facies cycles. In addition, two periods of accelerated subsidence were recognized, the first, in the Pliensbachian, drowned the platform, the second, prior to the late Bajocian, created accommodation space for resedimented carbonate deposits from the adjacent Friuli Carbonate Platform. The present day position of the succession is between the Belluno Basin to the west and the Slovenian Basin to the south. The hitherto described successions of these two basins were located more distally from the Friuli Carbonate Platform than the Mt. Mangart succession.

Riassunto. Al Mt. Mangart nelle Alpi Giulie affiora una successione Giurassica completa, che registra l'evoluzione dal margine della piattaforma sino a un bacino di acque profonde. La successione fa parte della Falda delle Giulie dove le Alpi meridionali sovrascorrono sulle Dinaridi. Durante il Giurassico, l'area faceva parte del margine continentale passivo della Tetide meridionale. La successione è stata studiata in dettaglio da un punto di vista sedimentologico e datata con i radiolari. È stata suddivisa in cinque unità litostratigrafiche: Unità 1: calcari a pelodi ed oncoidi di bassa profondità di età Giurassica inferiore; Unità 2: calcari di piattaforma distale ricchi di nuclei di ammoniti e

spicole di spugne, di età Pliensbachiana, sigillati da un hardground ricco in Fe-Mn; Unità 3: sequenza di argilliti nere con intercalazioni di calcari silicei di età Toarciana inferiore e forse media; Unità 4: selci, calcari con selce e accumuli carbonatici gravitativi di età da Bajociano/Bathoniano a Titoniano; Unità 5: calcari nodulari con selce del Titoniano superiore, con abbondanti calpionelle e aptichi. Una lacuna stratigrafica, dal Toarciano superiore al Bajociano inferiore, separa l'Unità 4 dall'Unità 3. In generale, la successione è ben confrontabile con i già noti cicli di trasgressione/regressione nella Tetide. Inoltre, si riconoscono due intervalli di subsidenza accelerata. Il primo, nel Pliensbachiano, portò all'annegamento della piattaforma. Il secondo, prima della fine del Bajociano superiore, permise il formarsi dello spazio per accogliere i carbonati risedimentati provenienti dalla Piattaforma Carbonatica Friulana adiacente. La posizione attuale è tra Bacino di Belluno ad ovest e Bacino Sloveno a sud, ma originariamente le successioni di questi due bacini si trovavano in posizione più distale rispetto alla successione del Mt. Mangart.

Introduction

The investigated section at Mt. Mangart is located in the Julian Alps, which comprise northwestern Slovenia and extend to the west, to the easternmost part of Italy (Fig. 1). In the Jurassic this region belonged to the passive continental margin of the southern Tethys and experienced extension due to rifting. Consequently, the relatively uniform Upper Triassic carbonate platform that comprised W Slovenia was dissected into blocks with different subsidence rates forming a horst-and-graben structure. The Jurassic subsidence history of southern Tethyan blocks is well documented westward, in the Southern Alps of Italy (Bosellini et al. 1981; Winterer & Bosellini 1981; Bernoulli et al. 1990; Bertotti 1991; Bertotti et al. 1993; Martire 1992, 1996) whereas in Slovenia information is scarce (Aubouin et al. 1965; Cousin 1970, 1981; Buser 1989, 1996).

¹ Paleontoloski institut Ivana Rakovca ZRC SAZU, Novi trg 2, SI-1000 Ljubljana, Slovenia. E-mail: smuc@zrc-sazu.si, spela@zrc-sazu.si

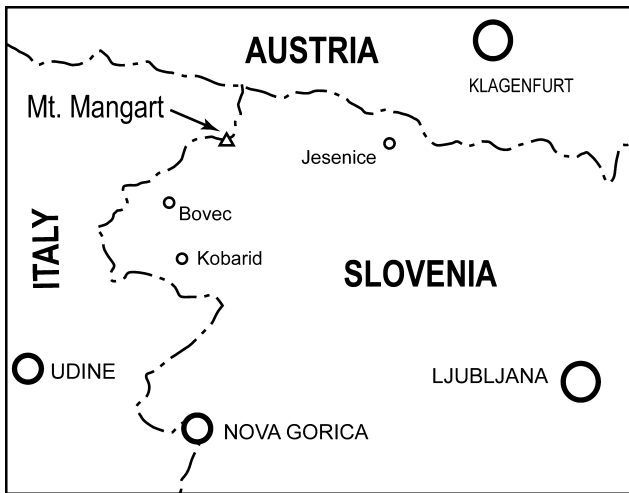


Fig. 1 - Geographic location of the studied area.

The succession at Mt. Mangart represents one of the best-preserved successions of uppermost Triassic to Lower Cretaceous strata in the Julian Alps and records rifting history and platform drowning. It is also important because it is located between the Belluno and Slovenian basins (Fig. 2) and provides new data to the paleogeographic relationship between these two basins that is still not satisfactorily resolved (see Aubouin et al. 1965; Cousin 1970, 1981; Bosellini et al. 1981; Winterer & Bosellini 1981; Buser 1996).

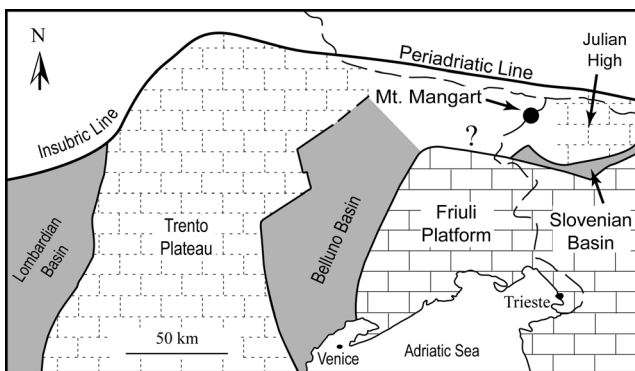


Fig. 2 - Present-day position of paleogeographic units and position of the studied area (modified from Winterer & Bosellini (1981) and Placer (1999)).

Few studies on Mt. Mangart have thus far been published. Cousin (1981) and Jurkovsek et al. (1990) mapped the Mt. Mangart area (Fig. 3). They also presented a composite stratigraphic section of the exposed Upper Triassic to Cretaceous formations. Jenkyns (1988) focused on a horizon of organic-rich shales with siliceous-limestone intercalations and interpreted these deposits as a product of the Toarcian Oceanic Anoxic Event. Recently, the Toarcian age of this horizon was confirmed using well-preserved and diverse radiolarian faunas (Goričan et al. 2003).

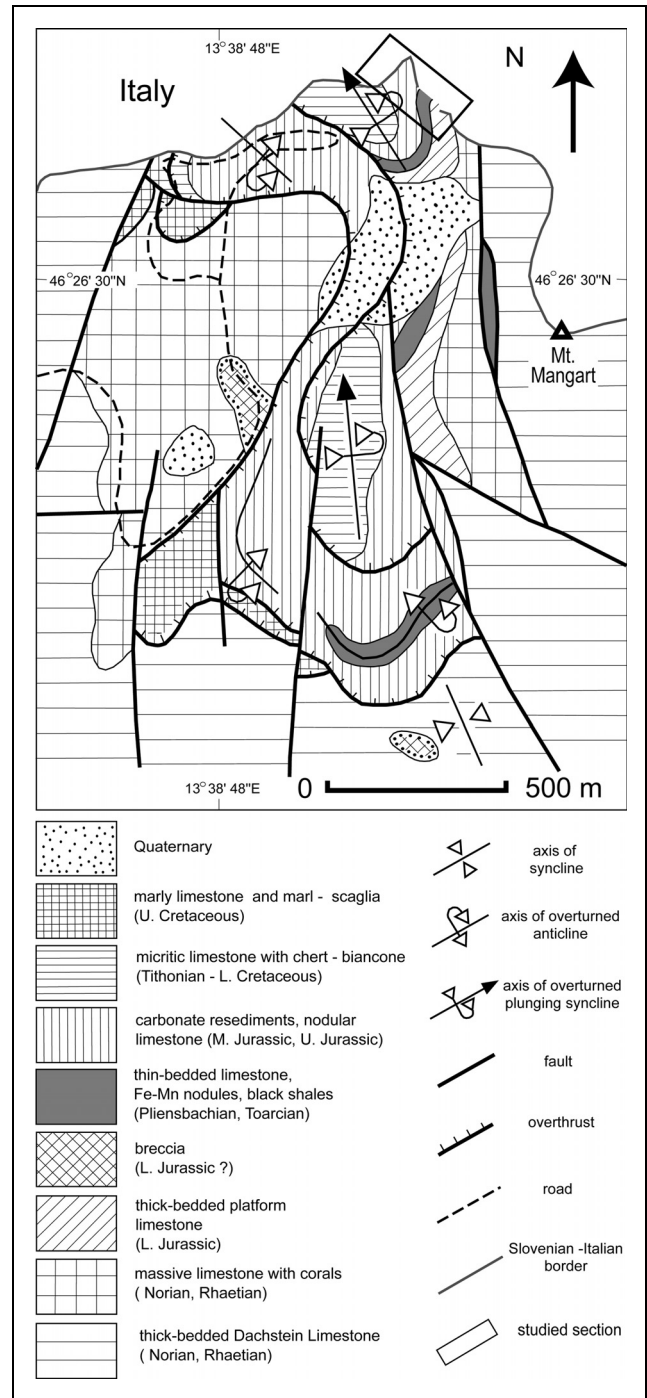


Fig. 3 - Geological map of the Mt. Mangart saddle (Jurkovsek et al. 1990) with the position of the studied section.

The aims of this paper are to:

- 1) present a detailed sedimentologic and biostratigraphic study of the Jurassic-lowermost Cretaceous succession at Mt. Mangart,
- 2) discuss the control of eustatic vs. tectonic factors on the observed depositional pattern, and
- 3) compare the sedimentary evolution of the Mt. Mangart area to the coeval evolution of the Belluno and Slovenian basins.

Geological setting

The Julian Alps are a part of a complex structure of western Slovenia formed mostly in the Cretaceous and in Tertiary during the Alpine orogeny (Placer 1999). The Julian Alps structurally belong to the Julian Nappe, which, together with the south-lying Tolmin Nappe, forms the eastern continuation of the Southern Alps (Placer 1999, fig. 1). In the Julian Alps, the Eocene or earlier, SW-directed (“Dinaric”) nappe emplacement is overprinted by the younger, Oligocene, south directed (“Southalpine”) thrusting (Doglioni & Bosellini 1987; Doglioni & Siorpaes 1990; Placer & Car 1998; Placer 1999).

The overall Mesozoic succession in the Julian Alps is characterized by a thick pile of shallow-water Upper Triassic to lower Lower Jurassic limestones overlain by condensed upper Lower Jurassic to Upper Cretaceous deeper-water sediments. Because of this stratigraphic situation, the inferred paleogeographic setting of this area (Fig. 2) during the late Early to Late Jurassic was thought to be a pelagic submarine high (Julian High in Buser 1996). The Julian High, however, was not a uniform plateau but was dissected into differentially subsided blocks. Some of these blocks became isolated pelagic carbonate platforms (*sensu* Santantonio 1994) while other blocks became a part of deeper basins receiving gravity-displaced material from the adjacent shallow-water platforms (as is the case at Mt. Mangart).

The Julian High was separated from the Friuli Carbonate Platform (Dinaric Carbonate Platform in Slovenian literature) by a deep basin, the Slovenian Basin (Cousin 1970). The pattern of these topographic highs and depressions distributed approximately in N-S direction is similar to the pattern recognized westward, where in the E-W direction we observe the Friuli Platform, Belluno Basin, and Trento Plateau (Fig. 2). The paleogeographic connection between the Belluno Basin and Slovenian Basin is still a matter of debate. Some authors (Aubouin et al. 1965; Cousin 1970, 1981; Buser 1996; Buser & Debeljak 1996) state that the Belluno and the Slovenian Basin did not form a physiographically uniform basin, but were both wedge-shaped and separated by a topographic high, while others (Bosellini et al. 1981; Winterer & Bosellini 1981; Bellanca et al. 1999; Clari & Masetti 2002) suggest that they were directly connected.

Mt. Mangart section: description of lithostratigraphic units

The Mt. Mangart section is exposed at the Slovenian-Italian border on the saddle between Travnik and Mali Mangart, near the footpath leading off the road

towards Veliki Mangart (46°26'80" N, 13°39'18" E, altitude 2164 m).

Detailed mapping of the Mt. Mangart saddle by Cousin (1981) and Jurkovek et al. (1990) revealed a complex tectonic structure of the area comprising three small-scale thrust sheets (Fig. 3). The studied section belongs to the topmost thrust sheet. The section is a part of an overturned syncline (Fig. 4a, b). We divided the section into five lithostratigraphic units (Fig. 5).

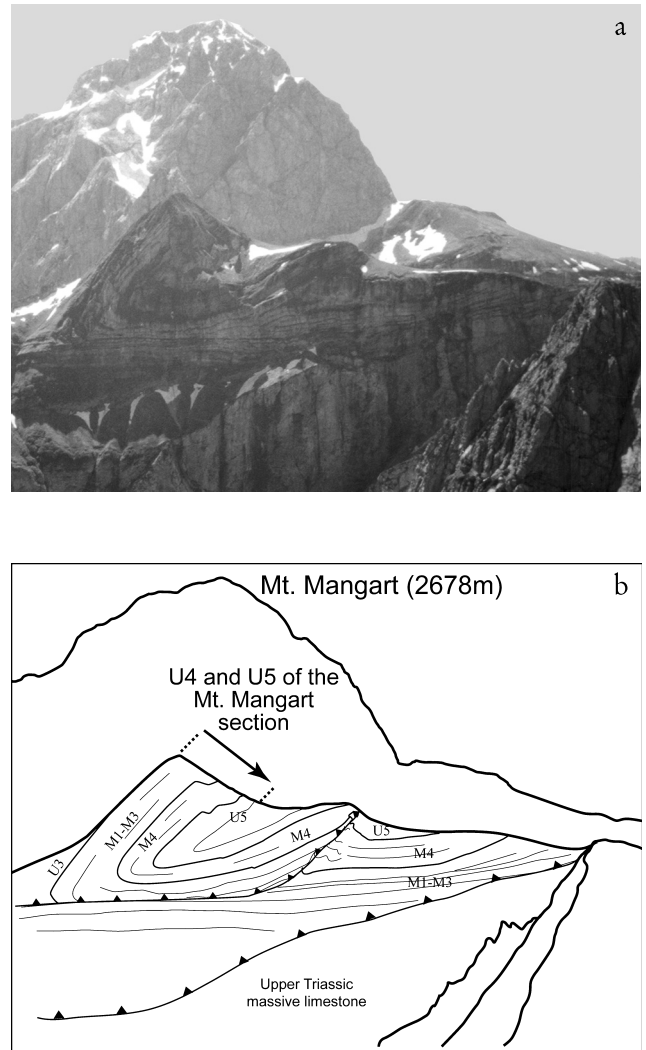


Fig. 4 - a View of the northern flank of Mt. Mangart. b - Structural sketch of the photograph in Fig. 4a. The three thrust sheets are clearly visible. The section belongs to the topmost thrust sheet, and was measured in an overturned syncline (for abbreviations of lithostratigraphic units see Fig. 5).

Unit 1 (U1) represents the base of the section and consists of lower Lower Jurassic shallow water peloidal and oncoidal limestone.

Unit 2 (U2, 27 m thick) is composed of Pliensbachian bioclastic limestones rich in echinoderms, juvenile ammonites, sponge spicules and foraminifers.

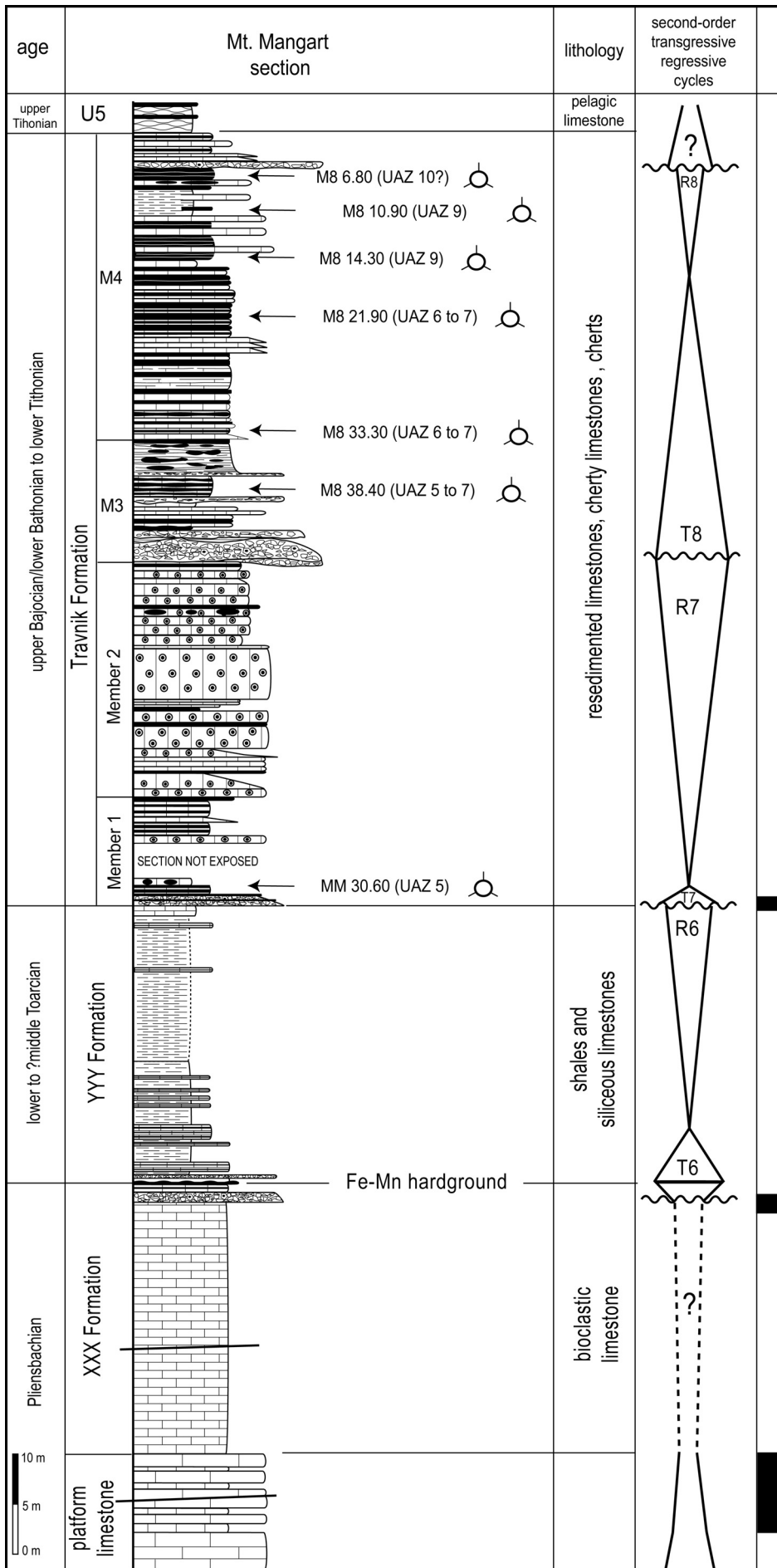




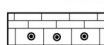


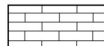
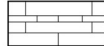






Fig. 5 - Mt. Mangart section with position of radiolarian samples (zonal assignment according to Baumgartner et al. (1995c) is indicated in brackets) and transgressive/regressive cycles (transgressive/regressive cycles are named according to Jacquín et al. (1998) and Graciansky et al. (1998)).

LEGEND:

-  pelagic limestone with calpionellids and chert
-  shales with intercalated calcarenites and siliceous mudstones
-  chert
-  - micritic limestone with chert nodules
- cherty limestone
- resedimented limestones**
 -  - calcarenites
 -  - ooid dominated calcarenites
 -  - carbonate breccia
-  shales and radiolarian-rich siliceous limestones
-  bioclastic wackestone with juvenile ammonites and sponge spicules
-  peloidal and oncoidal grainstone and intercalated peloidal packstone
-  times of increased tectonic subsidence
-  erosion
-  radiolarian samples in Unit 4

Unit 3 (U3, 27.5 m thick) consists of a lower Toarcian and possibly middle Toarcian sequence of black shales with interbedded dark gray siliceous limestone.

Unit 4 (U4, 77 m thick) is composed of upper Bajocian/Bathonian to lower Tithonian cherts, cherty limestones and carbonate gravity-flow deposits. On the basis of structure and composition of carbonate re-sediments, Unit 4 is subdivided into 4 members.

Unit 5 (U5) consists of upper Tithonian to lowermost Cretaceous red nodular cherty limestone with abundant calpionellids and aptychi.

Two discontinuity surfaces are recognized. The first one separates Pliensbachian bioclastic limestones (Unit 2) from the overlying lower Toarcian shales (Unit 3) and is evidenced by Fe-Mn nodules. The second surface is placed on the top of Unit 3, i.e. between the Toarcian shales of Unit 3 and upper Bajocian/Bathonian re-sedimented carbonates and cherts of Unit 4. This surface is characterized by intensive boring and corresponds to a significant stratigraphic break.

Unit 1: Peloidal and oncoidal limestone

Description. The dominant lithofacies is a light gray, massive, medium to well-sorted grainstone composed of non-skeletal and skeletal grains (Pl. 1, fig. 1). Non-skeletal grains are mainly intraclasts of peloidal wackestone/packstones and mudstones, peloids, micritized ooids and oncoids. The skeletal component consists of echinoderm fragments, gastropods, bivalves, spongiomorphids, fragments of algae and foraminifers. Grains are cemented first by bladed and syntaxial cements and then by coarser sparite.

In the uppermost part of the unit, up to 1 m thick beds of the above described grainstone alternate with up to 30 cm thick beds of a finer-grained wackestone/packstone (Pl. 1, fig. 2). Grains are peloids, rare ooids, benthic foraminifers (*Textulariidae*, *Valvulinidae*, *Lenticulina*, and *Agerina martana* (Farinacci)), rare echinoderms, and bivalves.

In the upper part of Unit 1 the presence of *Agerina martana* (Farinacci) (according to the biozonal scheme of Chiocchini et al. (1994)) suggests a Pliensbachian age. In the lower part of the section *A. martana* is not present so a Sinemurian age for this part of Unit 1 is possible.

Interpretation. Grainstones of the lower part of Unit 1 were deposited in a high-energy subtidal environment, most probably a sand belt in a marginal part of a shallow-water carbonate platform (cf. Di Stefano et al. 2002). The majority of grains originated from a subtidal lagoonal environment in the internal part of the shelf and were later transported to the platform margin.

The finer-grained peloidal wackestones/packstones intercalated in the upper part of the Unit 1 were deposited in hydrodynamically quieter environment located basinward from the marginal sandbelt. Deeper depositional environment is indicated by open marine elements (*Lenticulina*).

Unit 2: Bioclastic wackestone to packstone

Description. The boundary between the Unit 1 and the Unit 2 is sharp. The Unit 2 consists of light brownish-gray, massive or indistinctly bedded, and at places nodular (beds are up to 10 cm thick), bioclastic wackestone to packstone (Pl. 1, fig. 3a, 3b). The fossil content consists of sponge spicules, echinoderm fragments, locally abundant juvenile ammonites, and benthic foraminifers (*Textulariidae*, *Lenticulina*, *Agerina martana*), as well as rare ostracods and brachiopod shells. Glauconite is observed as small individual grains or as infilling in chambers of foraminifers. Pellets are abundant at places.

A distinctive 1 m thick greenish package occurs in the upper part of the Unit 2. It is composed of thin beds of poorly sorted, moderately to densely packed, normally graded, fine-grained breccia to coarse-grained calcarenite (Pl. 1, fig. 4). Elongate grains are oriented parallel to the bedding. Fragments of echinoderms and diverse intraclasts (mudstones, peloidal mudstones, bioclastic wackestones, and peloidal grainstones) are embedded in micritic and microsparitic matrix. Echinoderm grains show evidence of mechanical breakage and abrasion. Other grains are rare peloids, foraminifers (*Lenticulina*, *Agerina martana*), and bivalve fragments. Glauconite, chlorite and pyrite grains also occur within the matrix. In the outcrop this level is well distinguished from the underlying limestone by its darker color and increased clay content.

The uppermost 1.5 meters of the Unit 2 are composed of red siliceous limestone. The limestone is bedded, the beds are up to 10 cm thick and slightly nodular, the texture is wackestone/packstone with abundant, partly calcified, sponge spicules and radiolarians. Other grains are rare echinoderm fragments that are not present in the topmost beds of the Unit 2. The matrix is partly impregnated by Fe-Mn oxides. The siliceous limestone contains up to 3 cm large Fe-Mn nodules. They occur throughout the entire uppermost part of Unit 2 and are concentrated at the top of the unit forming a 25 cm thick bed composed exclusively of Fe-Mn nodules. The nodules mainly consist of quartz and pyrolusite and in minor content of cryptomelane, todorokite and goethite; the MnO content reaches up to 55% (Jurkovsek et al. 1990).

The common presence of *Agerina martana* (Farinacci) in the lower part of the Unit 2 suggests a Pliensbachian age. Because the overlying Unit 3 is early Toar-

cian in age (see below), the Fe-Mn hardground at the top of the Unit 2 corresponds approximately to the Pliensbachian/Toarcian boundary.

Interpretation. Bioclastic wackestones and packstones of the Unit 2 were deposited in low energy environment. Presence of open-marine biota (sponge spicules and juvenile ammonites) and absence of shallow-water elements suggest a deeper depositional environment compared to Unit 1, probably a distal shelf (cf. Elmi 1990).

Fine-grained breccias and coarse-grained calcarenites in the upper part of the unit are interpreted as gravity-flow deposits, as suggested by normal grading, relatively dense packing and parallel orientation of the elongate grains. The presence of completely lithified clasts of Unit 2 and Unit 1 indicates exhumation of underlying lithologies by synsedimentary extensional tectonics that produced unstable slope, uncovered older rocks and enabled erosion. The exhumed rocks were additionally eroded due to the mechanical abrasion by the grain-loaded turbulent water (cf. Di Stefano & Mindszenty 2000; Di Stefano et al. 2002).

In wackestones and packstones with ferromanganese nodules above the resedimented limestones, sponge spicules and radiolarians prevail and benthic calcareous organisms become scarce to absent. Extremely reduced sedimentation rates of these pelagic limestones is evidenced by Fe-Mn nodules. The sedimentation rate reached its minimum with the formation of the Fe-Mn hardground.

Unit 3: Shales with siliceous limestone

Description. In the lowermost part of the unit, a 40 cm thick bed of dark gray organic-rich, recrystallized wackestone/packstone occurs. It is composed of echinoderms, calcitized radiolarians, and sponge spicules.

Above the wackestone/packstone, a 10 cm thick bed of very poorly-sorted grain-supported fine-grained breccia is present. Normal grading is observed within the breccia bed. The breccia is composed mainly of echinoderm fragments and intraclasts. Rare foraminifers, fragments of bivalves and gastropods, glauconite, and phosphate grains are present. Intraclasts are made of mudstones and peloidal packstones. The breccia is cemented by drusy and syntaxial cement.

The breccia is overlain by black laminated calcareous organic-rich shales with interbedded black siliceous limestones. In the upper part of the unit, the shales are brown. The shales contain the minerals quartz, smectite and illite, and Mn oxides (Jenkyns 1988; Jurkovsek et al. 1990). The TOC values range between 0.48 and 1.7%. The manganese content is high (up to 9.27%) in the basal portion and decreases (1.12% or less) upsection (Jenkyns 1988).

The siliceous limestone (bed thickness up to 15 cm) intercalated within the shales varies from packstone to mudstone. In the lower part, beds are abundant and are mainly packstones and wackestones (Pl. 1, fig. 5). Towards the top of the unit, the beds of siliceous limestone become rare and are predominantly wackestones to mudstones. In the lower part of the unit, the siliceous limestone shows both normal and inverse grading, parallel and ripple cross-lamination, while upsection, only indistinct parallel lamination is present. The grain-to-matrix ratio and the mean size of radiolarians decrease upward. In the uppermost limestone beds, the grain-to-matrix proportion is again high (packstone/wackestone laminae). The limestone contains mainly radiolarians, sponge spicules (only in the lowermost part of the unit), intraclasts of lime mudstone (in the lowermost part of the unit only), and phosphate grains. Authigenic quartz and pyrite occur and are especially abundant in wackestone, while they are less common in the packstone beds. The matrix is micrite with high organic matter content.

Above the shale is a light green, thinly-bedded, laminated, recrystallized limestone that forms the top 0.90 m of Unit 3. Echinoderms, ostracods, foraminifers and calcitized radiolarians are very rare. Pyrite, limonite, quartz and glauconite are present. The limestone is intensively bored.

On the basis of radiolarians found in the intercalated siliceous limestone, we determined that Unit 3 is early Toarcian and possibly middle Toarcian in age (Gorican et al. 2003).

Interpretation. The entire Unit 3 records the high input of terrigenous clayey material. Black organic-rich shales in the lower part of the unit were deposited during the early Toarcian Oceanic Anoxic Event, as suggested by Jenkyns (1988) and confirmed with radiolarian dating (Gorican et al. 2003).

The limestone in the lowermost part of the unit is interpreted as hemipelagic limestone and indicates an increase in sedimentation rates following the formation of the Fe-Mn crust. Sedimentary structures and composition of the breccia bed are very similar to that in the breccia beds of Unit 2 and suggest a deposition by a high-density gravity-flow.

The sedimentary structures found in the siliceous limestone intercalated within shales are typical of fine-grained turbidites (e.g. Piper & Stow 1991). The nature of resedimented grains (only pelagic fauna) indicates redeposition of material within the sedimentary basin.

A stratigraphic gap, corresponding at least to the late Toarcian, Aalenian, and early Bajocian, separates Unit 3 from Unit 4. It was formed due to extremely slow sedimentation rates as evidenced by presence of extensive borings at the top of the Unit 3.

Unit 4: Resedimented limestones and siliceous sediments

Description. Unit 4 is composed of cherts, cherty limestones and carbonate gravity-flow deposits. On the basis of composition and sedimentologic features we divided Unit 4 into four members (Fig. 5).

Member M1 starts with a 1.3 m thick package of green, bedded (beds are up to 25 cm thick) fine-grained, poorly- to medium-sorted clast-supported breccia that grades into thin- to medium-bedded, coarse to medium-grained calcarenite. Breccia is composed mainly of lithoclasts and bioclasts: filaments, echinoderms, bivalve fragments, foraminifers (*Textulariidae*, *Lenticulina*), radiolarians and sponge spicules. Glauconite is abundant. The lithoclasts are composed of light gray limestone and siliceous limestone of the underlying Unit 3 and bioclastic wackestone/mudstone of Unit 2. The calcarenite is parallelly laminated, and elongate grains are aligned parallel to bedding. It has the same bioclasts as breccias, but contains more highly evolved glauconite grains (determined according to classification of Odin & Fullagar 1988) and it is devoid of lithoclasts. Some of the glauconite grains have fractured grain surface.

The overlying fine-grained rocks are thin-bedded gray siliceous limestone (packstone/wackestone) and dark gray laminated cherts that alternate with medium-bedded light gray homogenous wackestone with lenses of chert. The siliceous limestone shows parallel, low-angle cross lamination and wispy, convoluted lamination. Grains are partly calcitized radiolarians and rare fragments of echinoderms, and phosphate grains. The intercalated wackestone is composed of completely calcitized radiolarians and rare filaments. Rare, ooid bearing, beds (up to 30 cm thick) are interbedded in this interval.

Member M2 is characterized by 0.3 - 5 m thick beds of light gray oolitic packstone and grainstone (Fig. 6). Thicker beds are structureless while thinner (less than 0.5 m) beds at places show grading and parallel, and rarely ripple cross lamination. Limestones are composed mainly of ooids (Pl. 1, fig. 6). Other grains are echinoderms, peloids, foraminifers (*Textulariidae*, *Involutinidae*, *Lituolidae*), and micritic intraclasts. In some beds black chert nodules are present.

Member M3 begins with six, up to 2.60 m thick, carbonate breccia beds, each of them capped by fine-grained parallelly laminated limestone. The lowermost breccia bed lies within channel excavated into underlying M2. At places fine-grained calcarenites are missing and only amalgamated breccia beds are present. Breccias are grain-supported, graded and composed of up to 5 cm large lithoclasts of lithologies of members M2 and M1, and Unit 2 (Pl. 1, fig. 7). Other clasts are abundant fragments of echinoderms, fragments of stromatoporoids, corals and foraminifers (*Textulariidae*, *Involutinidae*, *Li-*



Fig. 6 - Unit 4: limestone megabeds (arrow) composed mainly of ooids: member M2 of Unit 4 (the section is in overturned position).

tuolidae). The overlying laminated fine-grained limestone is wackestone to packstone composed of filaments, small echinoderm fragments and micritized ooids.

This package is overlain by thin- to medium-bedded, coarse- to fine-grained limestones showing grading, parallel and wavy lamination (Ta-Tc Bouma divisions). They have similar composition as limestones of M2, but contain less ooids.

Thin-bedded, parallelly laminated radiolarian-bearing cherty limestone characterizes the middle part of the member M3.

Member M3 ends with a 3 m thick bed composed of 30 cm thick breccia at the base, which abruptly passes into massive fine-grained indistinctly laminated limestone with chert nodules. The breccia has the same composition as the breccias in the lower part of the member M3. The limestone with chert nodules ranges from packstone to wackestone composed of filaments, echinoderm fragments, rare ooids, phosphate grains and pyrite (Pl. 1, fig. 8).

Member M4 contains cherty limestones, cherts and siliceous mudstones with intercalations of fine to very coarse-grained calcarenites. Carbonate breccia is present in the uppermost part of the member.

The lower 15 m of member M4 are characterized by thin-bedded laminated (Td) black cherts and cherty limestones (same composition as cherty limestones of M3) with intercalated thin-bedded, fine to coarse-grained calcarenites. Calcarenites show Ta-b and Tb-d Bouma divisions and are packstones composed of filaments, peloids, echinoderm fragments, foraminifers (*Textulariidae*, *Involutinidae*, *Lituolidae*) and phosphate grains. Ooids are rare. In coarse-grained facies, reworked lithoclasts of M1, M2, and M3 occur. In the middle part of member M4, thin beds of orange replacement chert are present.

The upper part of the member M4 (at sample M8 14.30) starts with red radiolarian cherts with intercalated coarse to very coarse-grained calcarenites (Ta Bouma divisions), and continues with a 2.5 meter thick clay-rich package containing intercalations of red calcareous clay-rich chert and coarse-grained calcarenites. The uppermost part of M4 is composed of red radiolarian-rich marls with intercalations of a carbonate breccia and coarse-grained calcarenites. The intercalated coarse-grained calcarenites are packstones to grainstones composed of peloids, echinoderm grains, foraminifers (Textulariidae, Involutinidae), rare small ooids and mudstone clasts. In the uppermost part of the Member 4 the calcarenites are composed exclusively of echinoderm fragments.

The breccia bed (30 cm thick) in the upper part of M4 is coarse-grained (clasts are up to 10 cm), grain-supported and composed mainly of large lithoclasts of underlying lithologies of Unit 4. Other grains are echinoderms, belemnites, peloids, foraminifers (Textulariidae, Valvulinidae), fragments of algae and corals. Important constituents are rare but large (up to 2 mm) euhedral detritic grains of bytownite-anorthite feldspars.

Unit 4 was dated with radiolarians. It ranges from the upper Bajocian to lower Tithonian. Ages of individual samples are discussed separately in the next chapter.

Interpretation. Unit 4 was deposited in a deeper basin that was directly connected to the adjacent carbonate platform. Homogenous wackestones, cherts, and calcareous clayey cherts constitute the background sedimentation. Fine-grained siliceous limestones show sedimentary characteristics that indicate hydrodynamic sorting of material and probably deposition by low-density turbidity currents. Medium to fine-grained limestones exhibit Bouma sequences, with base-cut-out sequences being the most frequent. This indicates that through most of Unit 4 time, the depositional setting was a lower slope or basin plain. Oolitic megabeds in M2 are continuous at the outcrop scale and their thickness is laterally constant. In addition, oolitic megabeds are associated with finer-grained turbidites. Their position in the basin was thus relatively distal as well. The most proximal deposits of Unit 4 are channelized and often amalgamated breccia beds at the base of the M3 member. Individual breccia beds are directly overlain by fine-grained calcarenites interpreted to be the dilute "tail" of the same gravity flow that produced each breccia bed, thus indicating substantial sediment bypass (cf. Mutti 1992).

The composition of limestone reveals that most of the grains result from penecontemporaneous carbonate production supplied from the marginal parts of the adjacent platform. The coarser-grained beds include litho-

clasts of older basinal sediments and thus indicate partial erosion of underlying deposits. The basal breccias and calcarenites of M1, in addition, contain highly evolved glauconite grains that indicate long sediment starvation in the provenance area (Odin & Fullagar 1988; Amorosi 1995). Clasts of older pelagic rocks are the largest and prevail over other constituents in the breccia bed of M4. This breccia was probably deposited relatively close to an escarpment produced by normal faulting.

Unit 5: Red nodular cherty limestone

Unit 5 consists of red nodular (bed thickness is up to 5 cm) mudstone/wackestone composed mainly of calpionellids (including *Crassicollaria* sp. and *Calpionella alpina* (Lorenz)), aptychi, and calcitized radiolarians. Beds (up to few centimeters thick) of red replacement chert occur within nodular limestones.

The occurrence of *Crassicollaria* sp. and *Calpionella alpina* suggests that limestones are not older than late Tithonian (according to Remane 1985 and Grün & Blau 1997). At the Mt. Mangart section, the overlying beds are extensively folded and could not be logged.

Radiolarian dating

The siliceous-limestone intercalations of Unit 3 contain diverse and well preserved radiolarian faunas, which indicate an early and possibly middle Toarcian age. Systematics, age assignment and paleoecological implications of these faunas have already been presented in detail (Goričan et al. 2003).

In this chapter we discuss the radiolarian content of Unit 4. Seven productive samples (for stratigraphic position see Fig. 5) were analyzed. The samples MM 30.60 and M8 14.30 are radiolarian cherts and were treated only with diluted 9% hydrofluoric acid. The other samples contain some carbonate; these were treated first with acetic and then with HF acid. The sample M8 21.90 revealed moderately-well preserved radiolarians after both treatments, while in samples M8 38.40, M8 33.30, M8 10.90, and M8 6.80 determinable radiolarians were obtained only after HF attack. In all samples nassellarians are much more abundant than spumellarians, spumellarians are relatively common only in the acetic-acid residue of the M8 21.90 sample.

The assemblages were dated with the zonation of Baumgartner et al. (1995c), who established 22 Unitary Association Zones (UAZ) for the Middle Jurassic to Early Cretaceous time interval. The species inventory is given in Table 1 and illustrated in Pl. 2 to 4.

Rock samples, residues and photographed radiolarian specimens are stored at the Ivan Rakovec Insti-

Species	Samples	UAZ95	MM 30.60	M8 38.40	M8 33.30	M8 21.90	M8 14.30	M8 10.90	M8 6.80
<i>Angulobracchia biordinalis</i> Ozvoldova (Pl. 2, fig. 12)		9-11						x	
<i>Archaeodictyomitra ? amabilis</i> Aita (Pl. 4, fig. 3)		4-7		x	x				
<i>Archaeodictyomitra apiarium</i> (Rüst) (Pl. 4, fig. 6)		8-22					x		x
<i>Archaeodictyomitra minoensis</i> (Mizutani) (Pl. 4, figs. 7-8)		9-12					x	x	
<i>Bernoullius dicera</i> (Baumgartner) (Pl. 2, fig. 15)		3-10						x	
<i>Cinguloturris carpatica</i> Dumitrica (Pl. 4, fig. 22)		7-11					x	x	
<i>Cryptamphorella</i> spp. (Pl. 3, figs. 31a-b, 32a-c)									x
<i>Deviatus diampheids</i> (Foreman) s.l. (Pl. 2, fig. 11)		8-22						x	
<i>Dicerosaturnalis trizonalis angustus</i> (Baumgartner) (Pl. 2, figs. 9-10)		6-10					x		x
<i>Dictyomitrella ? kamoensis</i> Mizutani & Kido (Pl. 4, figs. 27-28)		3-7	x		x	x			
<i>Eucyrtidiellum nodosum</i> Wakita (Pl. 2, fig. 23)		3-10					x		
<i>Eucyrtidiellum ptyctum</i> (Riedel & Sanfilippo) (Pl. 2, figs. 26-28)		5-11				x	x	x	
<i>Eucyrtidiellum semifactum</i> Nagai & Mizutani (Pl. 2, figs. 24-25)		5-7	x		x				
<i>Eucyrtidiellum unumaense pustulatum</i> Baumgartner (Pl. 2, figs. 21-22)		5-8			x	x	x		
<i>Fultacapsa sphaerica</i> (Ozvoldova) (Pl. 2, fig. 19)		9-11							x
<i>Gongylothorax favosus</i> Dumitrica (Pl. 3, fig. 26)		8-10					x	x	
<i>Gongylothorax ponticus</i> Bragin & Tekin (Pl. 3, figs. 4a-b, 5)					x	x			
<i>Gongylothorax</i> sp. A (Pl. 3, figs. 27-28, 29a-b, 30a-c)									x
<i>Guexella nudata</i> (Kocher) (Pl. 3, fig. 3)		5-8			x	x			
<i>Hexasaturnalis suboblongus minor</i> (Baumgartner) (Pl. 2, figs. 6-8)		3-11					x	x	x
<i>Hexasaturnalis suboblongus</i> ssp. A (Pl. 2, figs. 3-5)				x		x			x
<i>Hexasaturnalis suboblongus suboblongus</i> (Yao) (Pl. 2, fig. 2)		3-11	x						
<i>Hexasaturnalis</i> cf. <i>tetraspinus</i> (Yao) (Pl. 2, fig. 1)		1-6	x						
<i>Higumastra imbricata</i> (Ozvoldova) (Pl. 2, fig. 16)		4-8				x			
<i>Hsuum rutogense</i> Yang & Wang (Pl. 4, figs. 1-2)					x	x			
<i>Kilinora spiralis</i> (Matsuoka) (Pl. 2, fig. 42)		6-7				x			
<i>Levilugeo ordinarius</i> Yang & Wang (pl. 2, fig. 17)						x			
<i>Loopus doliolum</i> Dumitrica (Pl. 4, fig. 29)								x	
<i>Palinandromeda podbielensis</i> (Ozvoldova) (Pl. 2, fig. 20)		5-9					x		
<i>Parahsuum carpathicum</i> Widz & De Wever (Pl. 4, figs. 4-5)								x	
<i>Podobursa rosea</i> Hull (Pl. 2, fig. 30)						x			
<i>Podobursa triacantha</i> (Fischli) (Pl. 2, fig. 29)						x	x	x	x
<i>Praecaneta</i> spp. (Pl. 4, fig. 30)							x	x	
<i>Protunuma japonicus</i> Matsuoka & Yao (Pl. 2, figs. 36-37)		7-12					x	x	
<i>Protunuma ? aff. ianosus</i> Ozvoldova (Pl. 2, fig. 35)						x			
<i>Protunuma ? ochiensis</i> Matsuoka (Pl. 2, figs. 33a-b)		5-14			x				
<i>Pseudoristola tsunoensis</i> (Aita) (Pl. 3, figs. 15a-b, 16a-b)		6-7				x			
<i>Pseudodictyomitrella</i> spp. (Pl. 4, figs. 25-26)					x	x	x	x	
<i>Ristola altissima altissima</i> (Rüst) (Pl. 4, fig. 36)		7-12					x	x	
<i>Ristola altissima major</i> Baumgartner & De Wever (Pl. 4, fig. 35)		5-7		x	x				
<i>Stichocapsa convexa</i> Yao (Pl. 3, figs. 6-7)		1-11	x		x	x			
<i>Stichocapsa robusta</i> Matsuoka (Pl. 3, figs. 11-12)		5-7		x	x	x			
<i>Stichomitra ? annibill</i> Kocher (Pl. 4, fig. 24)						x			
<i>Stichomitra ? tairai</i> Aita (Pl. 4, fig. 23)						x			
<i>Striatojaponocapsa conexa</i> (Matsuoka) (Pl. 2, figs. 40-41)		4-7	x	x	x	x			
<i>Striatojaponocapsa ? matsukoai</i> (Sashida) (Pl. 2, figs. 43a-b)					x	x			
<i>Striatojaponocapsa plicarum plicarum</i> (Yao) (Pl. 2, figs. 38a-b, 39)		4-5	x						
<i>Stylocapsa ? catenarum</i> Matsuoka (Pl. 3, fig. 2)		6-7			x				
<i>Stylocapsa oblongula</i> Kocher (Pl. 3, fig. 23)		6-8			x	x			
<i>Tethysetta dhimenaensis</i> (Baumgartner) s.l. (Pl. 4, fig. 31)		3-11		x	x	x	x	x	
<i>Tetratrabs bulbosa</i> Baumgartner		7-11						x	
<i>Tetratrabs zealis</i> (Ozvoldova) (Pl. 2, fig. 14)		4-13		x		x	x	x	
<i>Theocapsomma medvednicensis</i> Gorican (Pl. 3, fig. 1)					x				
<i>Transsuum brevicostatum</i> (Ozvoldova) gr. (Pl. 4, figs. 10-14)		3-11			x		x	x	
<i>Transsuum maxwellii</i> (Pessagno) gr. (Pl. 4, fig. 9)		3-10	x						
<i>Triactoma blakei</i> (Pessagno) (Pl. 2, fig. 18)		4-11						x	
<i>Tritrabs casmaliensis</i> (Pessagno) (Pl. 2, fig. 13)		4-10				x		x	
<i>Triversus ?</i> spp. (Pl. 4, figs. 32-33)						x			
<i>Unuma damoensis</i> Kozur (Pl. 2, fig. 32)			x						
<i>Unuma gordus</i> Hull (Pl. 2, fig. 34)		4-6		x	x	x			
<i>Unuma latusicostatus</i> (Aita) (Pl. 2, fig. 31)		4-5	x						
<i>Williriedellum carpathicum</i> Dumitrica (Pl. 3, fig. 20)		7-11					x	x	
<i>Williriedellum crystallinum</i> Dumitrica (Pl. 3, fig. 17)		7-11					x	x	
<i>Williriedellum marcucciae</i> Cortese (Pl. 3, figs. 21a-b)		4-8			x	x			
<i>Williriedellum yahazuense</i> (Aita) (Pl. 3, fig. 19)							x		
<i>Williriedellum yaoi</i> (Kozur) (Pl. 3, figs. 24a-b, 25a-b)				x		x	x		
<i>Xitus magnus</i> Baumgartner (Pl. 4, fig. 21)		8-11					x	x	
<i>Xitus skenderbegi</i> (Chiari, Marcucci & Prella) (Pl. 4, figs. 15-16)				x	x				
<i>Xitus</i> spp. (Pl. 4, figs. 17-20)			x	x	x		x	x	
<i>Zhamoidellum ovum</i> Dumitrica (Pl. 3, figs. 8a-b, 9-10)		9-11			x		x	x	
<i>Zhamoidellum ventricosum</i> Dumitrica (Pl. 3, figs. 13, 14a-b)		8-11				x		x	
Age (UAZones 95)			5	5-7	6-7	6-7	9	9	10 ?

Tab. 1 - Occurrence of radiolarian species in the samples studied. The first column gives zonal ranges of species according to Baumgartner et al. (1995c), the zonal assignment of the samples is shown in the bottom row.

tute of Palaeontology, Scientific Research Centre of the Slovenian Academy of Sciences and Arts.

Sample MM 30.60: dark gray laminated chert; radiolarians poorly preserved, relatively large sponge spicules common. The assemblage corresponds to UAZ 5 (latest Bajocian – early Bathonian). This zonal assignment is indicated by co-occurrence of *Eucyrtidium semifactum* (FAD in UAZ 5) and *Unuma latusicostatus* (LAD in UAZ 5). Among other species, *Unuma darnoensis* also seems to be stratigraphically important. It was recorded by Goričan (1994) in UAs 6 to 8, which are approximately correlative to UAZs 4 to 5 (late Bajocian to early Bathonian) of Baumgartner et al. (1995c, p. 1037).

Sample M8 38.40: black cherty limestone; radiolarians poorly preserved, rare tetraxone and monaxone spicules co-occur. Only a broad age assignment to UAZs 5 to 7 (latest Bajocian-early Bathonian to late Bathonian-early Callovian) is possible on the basis of *Archaeodictyomitra? amabilis*, *Ristola altissima major*, and *Stichocapsa robusta*. *Unuma gordus*, by Baumgartner et al. (1995c) supposed to be restricted to UAZs 4 to 6, was also found in overlying samples M8 33.30 and M8 21.90, and probably has a longer range than previously thought.

Sample M8 33.30: laminated gray limestone with black replacement chert; radiolarians poorly preserved; monaxone and tetraxone sponge spicules rare, rhaxes very rare. The assemblage is assignable to UAZs 6 to 7 (middle Bathonian to late Bathonian-early Callovian) based on the range of *Stylocapsa? catenarum*, FAD of *Stylocapsa oblongula* in UAZ 6, and LAD of several species in UAZ 7 (Table 1). *Zhamoidellum ovum* (Pl. 3, figs. 8a-b) co-occurs, suggesting that the proposed range of this species (UAZs 9 to 11) should be extended down to the Middle Jurassic.

Sample M8 21.90: gray limestone with small nodules of black chert; radiolarian fauna moderately-well preserved but relatively diverse; monaxone and tetraxone sponge spicules common. The stratigraphically most important species is *Kilinora spiralis*, which is rather common in this sample. Its range is restricted to UAZs 6 to 7. Several characteristic species, which last appear in UAZ 7 are present (e.g. *Striatojaponocapsa conexa*, *Dictyomitrella? kamoensis*, *Stichocapsa robusta*), the sample is thus certainly not younger than early Callovian. Because the age assignment is the same as for the previous sample, it seems probable that the sample M8 21.90 belongs to the upper part of the determined time interval.

Sample M8 14.30: violet red bedded chert, radiolarians moderately-well preserved; sponge spicules common, relatively large. The age is constrained with *Archaeodictyomitra minoensis* and *Palinandromeda podbielensis*, which co-exist in UAZ 9 (middle-late Ox-

fordian). *Eucyrtidiellum unumaense pustulatum*, confined to UAZ 8 and older zones is also present.

Sample M8 10.90: red laminated calcareous clay-rich chert; radiolarians abundant, relatively well-preserved and diverse; sponge spicules rare. The species inventory is similar to that of the previous sample. The assemblage is assignable to UAZs 9 to 10 (FADs of *Angulobracchia biordinalis* and *Archaeodictyomitra minoensis* in UAZ 9, LADs of *Bernoullius dicera*, *Gonylothorax favosus*, and *Tritrabs casmaliaensis* in UAZ 10). In the zonation of Goričan (1994), the assemblage corresponds to the union of UA 19 to UA 22, that are correlative with the UAZ 9 (Baumgartner et al. 1995c, p. 1037). The most probable age is thus UAZ 9 (middle-late Oxfordian).

Sample M8 6.80: red radiolarian-rich marl; radiolarians fairly-well preserved, diversity very low, assemblage dominated by cryptocephalic and cryptothoracic nassellarians; sponge spicules diverse, relatively large, more abundant than radiolarians. The high abundance of cryptocephalic nassellarians (see Zügel et al. 1998) as well as the proportion of sponge spicules (see Kiessling 1996) indicate a shift to more proximal basin facies in the last few meters of Unit 4. Because of observed very low diversity, a precise age assignment is rather difficult. The presence of *Dicerosaturnalis trizonalis angustus* suggests that this assemblage is not younger than UAZ 10 (late Oxfordian – early Kimmeridgian). The sample is certainly not younger than early Tithonian as evidenced by *Hexasaturnalis suboblongus minor* and *Fultacapsa sphaerica* (LADs in UAZ 11) as well as by the stratigraphic position below the limestone with calpionellids.

Notes to systematics

Basic synonymy is provided for the species which are not included in the catalogue of Baumgartner et al. (1995a) and short remarks are given for the species in open nomenclature. The taxa are listed in alphabetical order.

PLATE 1

Microfacies of the Mt. Mangart section. Scale bar in all pictures is 1 mm long, except Fig. 3b, where scale bar is 0,1mm long.

- Fig. 1 - Unit 1: grainstone with peloids, oncoids, bioclasts and intraclasts.
- Fig. 2 - Upper part of Unit 1: packstone with smaller peloids, intraclasts and small benthic foraminifera (*Agerina martana* (Farinacci) in the upper left corner of the picture, marked with arrow).
- Fig. 3a - Unit 2: wackestone with juvenile ammonites, sponge spicules, echinoderm fragments and *Agerina martana* (Farinacci).
- Fig. 3b - Unit 2: close up of Fig. 3a showing *Agerina martana* (Farinacci).

- Fig. 4 - Upper part of Unit 2: carbonate breccia composed mainly of echinoderm debris and diverse intraclasts (intraclast of peloidal grainstone in the middle of the picture).
- Fig. 5 - Unit 3: graded siliceous limestone with radiolarians and rare micritic intraclasts,
- Fig. 6 - Unit 4, Member 2: grainstone with ooids, peloids, micritic intraclasts and echinoderms.
- Fig. 7 - Unit 4, Member 3: carbonate breccia with lithoclasts of mudstones with radiolarians of M1, and bioclastic wackestone of Unit 2 (in the upper right corner of the picture).
- Fig. 8 - Unit 4, top of Member 3: massive fine-grained partly silicified wackestone with radiolarians.
- Fig. 29 - *Podobursa triacantha* (Fischli), M8 10.90, 031035, 150x.
- Fig. 30 - *Podobursa rosea* Hull, M8 21.90, 030605, 150x.
- Fig. 31 - *Unuma laticostatus* (Aita), MM 30.60, 023314, 200x.
- Fig. 32 - *Unuma darnoensis* Kozur, MM 30.60, 023312, 200x.
- Figs. 33 a-b - *Protunuma? ochiensis* Matsuoka, M8 33.30. Fig. 33a) 030406; Fig. 33b) antapical view, 030407; 200x.
- Fig. 34 - *Unuma gordus* Hull, M8 33.30, 030411, 200x.
- Fig. 35 - *Protunuma? aff. lanosus* Ozvoldova, M8 21.90, 030804, 200x.
- Figs. 36-37 - *Protunuma japonicus* Matsuoka & Yao, M8 14.30. Fig. 36) 020235; Fig. 37) 020201; 200x.
- Figs. 38 a-b, 39- - *Striatojaponocapsa plicarum plicarum* (Yao), MM 30.60. Fig. 38a) 023316; Fig. 38b) antapical view, 023317; Fig. 39) 023322; 200x.
- Figs. 40-41 - *Striatojaponocapsa conexa* (Matsuoka), M8 33.30. Fig. 40) 030413; Fig. 41) 030416; 200x.
- Fig. 42 - *Kilinora spiralis* (Matsuoka), M8 21.90, 030718, 200x.
- Figs. 43 a-b - *Striatojaponocapsa? matsukoi* (Sashida), M8 21.90. Fig. 43a) 030630; Fig. 43b) antapical view, 030629; 200x.

PLATE 2

Radiolarians from Unit 4 of Mt. Mangart section. For each illustration the sample number, SEM negative number, and magnification are indicated.

- Fig. 1 - *Hexasaturnalis cf. tetraspinus* (Yao), MM 30.60, 023329, 150x.
- Fig. 2 - *Hexasaturnalis suboblongus suboblongus* (Yao), MM 30.60, 023328, 150x.
- Figs. 3-5 - *Hexasaturnalis suboblongus* ssp. A. Fig. 3) M8 38.40, 030220; Fig. 4) M8 21.90, 030522; Fig. 5) M8 6.80, 031111; 150x.
- Figs. 6-8 - *Hexasaturnalis suboblongus minor* (Baumgartner). Fig. 6) M8 14.30, 020224; Fig. 7) M8 10.90, 030803; Fig. 8) M8 6.80, 031112; 150x.
- Figs. 9-10 - *Dicerosaturnalis trizonalis angustus* (Baumgartner). Fig. 9) M8 6.80, 031114; Fig. 10) M8 14.30, 020225; 150x.
- Fig. 11 - *Deviatus diamphidius* (Foreman) s.l., M8 10.90, 030832, 150x.
- Fig. 12 - *Angulobracchia biordinalis* Ozvoldova, M8 10.90, 030902, 100x.
- Fig. 13 - *Tritrabs casmaliaensis* (Pessagno), M8 21.90, 030533, 150x.
- Fig. 14 - *Tetratrabs zealis* (Ozvoldova), M8 38.40, 030222, 100x.
- Fig. 15 - *Bernoullius dicera* (Baumgartner), M8 10.90, 030831, 200x.
- Fig. 16 - *Higumastra imbricata* (Ozvoldova), M8 21.90, 030525, 100x.
- Fig. 17 - *Levileugeo ordinarius* Yang & Wang, M8 21.90, 030528, 150x.
- Fig. 18 - *Triactoma blakei* (Pessagno), M8 10.90, 030905, 100x.
- Fig. 19 - *Fultacapsa sphaerica* (Ozvoldova), M8 6.80, 031122, 150x.
- Fig. 20 - *Palinandromeda podbielensis* (Ozvoldova), M8 14.30, 020219, 100x.
- Figs. 21-22 - *Eucyrtidiellum unumaense pustulatum* Baumgartner. Fig. 21) M8 33.30, 030512; Fig. 22) M8 14.30 020121; 200x.
- Fig. 23 - *Eucyrtidiellum nodosum* Wakita, M8 14.30, 020124, 200x.
- Figs. 24-25 - *Eucyrtidiellum semifactum* Nagai & Mizutani. Fig. 24) MM 30.60, 023315; Fig. 25) M8 33.30, 030401, 200x.
- Figs. 26-28 - *Eucyrtidiellum ptyctum* (Riedel & Sanfilippo). Fig. 26) M8 21.90, 030713; Fig. 27) M8 14.30, 02122; Fig. 28) M8 10.90, 030909; 200x.

PLATE 3

Radiolarians from Unit 4 of Mt. Mangart section. For each illustration the sample number, SEM negative number, and magnification are indicated.

- Fig. 1 - *Theocapsomma medvednicensis* Gorican, M8 33.30, 030428, 200x.
- Fig. 2 - *Stylocapsa? catenarum* Matsuoka, M8 33.30, 030334, 300x.
- Fig. 3 - *Guxella nudata* (Kocher), M8 33.30, 030328, 200x.
- Figs. 4 a-b, 5 - *Gongyloborax ponticus* Bragin & Tekin. Figs. 4 a-b) M8 33.30, Fig. 4a) 030519, Fig. 4b) antapical view, 030518; Fig. 5) M8 21.90, 030725; 200x.
- Figs. 6-7 - *Stichocapsa convexa* Yao, Fig. 6) MM 30.60, 023332; Fig. 7) M8 21.90, 030811; 200x.
- Figs. 8 a-b, 9-10 - *Zhamoidellum ovum* Dumitrica. Fig. 8) M8 33.30, Fig. 8a) 030506, Fig. 8b) antapical view, 030507; Fig. 9) M8 14.30, 020214; Fig. 10) M8 10.90, 030920; 200x.
- Figs. 11-12 - *Stichocapsa robusta* Matsuoka. Fig. 11) M8 38.40, 030232; Fig. 12) M8 21.90, 030701; 200x.
- Figs. 13, 14a-b - *Zhamoidellum ventricosum* Dumitrica, M8 21.90. Fig. 13) 030628; Fig. 14a) 030729, Fig. 14b) antapical view, 030728; 200x.
- Figs. 15 a-b, 16 a-b - *Pseudoristola tsunoensis* (Aita), M8 21.90. Fig. 15a) 030615; Fig. 15b) antapical view, 030616; Fig. 16a) 030733; Fig. 16b) antapical view, 030732; 200x.
- Fig. 17 - *Williriedellum crystallinum* Dumitrica, M8 14.30, 020208, 200x.
- Fig. 18 - *Williriedellum cf. yabazuense* (Aita), M8 14.30, 020209, 200x.
- Fig. 19 - *Williriedellum yabazuense* (Aita), M8 14.30, 020236, 200x.
- Fig. 20 - *Williriedellum carpathicum* Dumitrica, M8 14.30, 020222, 200x.
- Figs. 21 a-b - *Williriedellum marcucciae* Cortese, M8 33.30. Fig. 21a) 030428; Fig. 21b) antapical view, 030427; 200x.
- Figs. 22 a-b - *Stichocapsa* sp., M8 21.90. Fig. 22a) 030711, Fig. 22b) antapical view, 030712; 200x.
- Fig. 23 - *Stylocapsa oblongula* Kocher, M8 33.30, 030515, 300x.

- Figs. 24 a-b, - *Williriedellum yaoi* (Kozur). Fig. 24a) M8 38.40, 25 a-b 030224; Fig. 24b) antapical view, 030223; Fig. 25a) M8 14.30, 020212; Fig. 25b) antapical view, 020214; 200x.
- Fig. 26 - *Gongylothorax favosus* Dumitrica, M8 10.90, 030926, 200x.
- Figs. 27-28, - *Gongylothorax* sp. A, M8 6.80. Fig. 27) 031218; Fig. 29 a-b, 30 a-c 28) 031134; Fig. 29a) 031221; Fig. 29b) antapical view, 031219; Fig. 30a) 031209; Fig. 30b) antapical view, 031208; Fig. 30c) apical view, 031207; 200x.
- Figs. 31 a-b, - *Cryptamphorella* spp., M8 6.80. Fig. 31a) 031201; 32 a-c Fig. 31b) apical view, 031203; Fig. 32a) 031215; Fig. 32b) antapical view, 031214; Fig. 32c) apical view, 031213; 200x.
- Fig. 9 - *Transhsuum maxwelli* (Pessagno) gr., MM 30.60, 020308, 200x.
- Figs. 10-14 - *Transhsuum brevicostatum* (Ozvodova) gr. Fig. 10) M8 33.30, 030308; Fig. 11) M8 10.90, 031016; Fig. 12) M8 10.90, 031014; Fig. 13) M8 14.30, 020234; Fig. 14) M8 14.30, 020109; 200x.
- Figs. 15-16 - *Xitus skenderbegi* (Chiari, Marcucci & Prela). Fig. 15) M8 38.40, 030204; Fig. 16) M8 33.30, 030313; 200x.
- Figs. 17-20 - *Xitus* spp. Fig. 17) M8 33.30, 030314; Fig. 18) M8 14.30, 020111; Fig. 19) M8 10.90, 031015; Fig. 20) M8 14.30, 020101; 200x.
- Fig. 21 - *Xitus magnus* Baumgartner, M8 10.90, 031021, 150x.
- Fig. 22 - *Cinguloturris carpatica* Dumitrica, M8 14.30, 020125, 200x.
- Fig. 23 - *Stichomitra? tairai* Aita, M8 21.90, 030609, 200x.
- Fig. 24 - *Stichomitra? annibill* Kocher, M8 21.90, 030806, 200x.
- Figs. 25-26 - *Pseudodictyomitrella* spp. Fig. 25) M8 10.90, 031034; Fig. 26) M8 14.30, 020130; 200x.
- Fig. 27-28 - *Dictyomitrella? kamoensis* Mizutani & Kido, MM 30.60. Fig. 27) 023304; Fig. 28) 023306; 200x.
- Fig. 29 - *Loopus doliolum* Dumitrica, M8 10.90, 031013, 200x.
- Fig. 30 - *Praecaneta* sp., M8 10.90, 031027, 200x.
- Fig. 31 - *Tethysetta dhimenaensis* (Baumgartner) s.l., M8 14.30, 020233, 200x.
- Figs. 32-33 - *Triversus? spp.*, M8 21.90. Fig. 32) 030631; Fig. 33) 030821; 200x.
- Fig. 34 - *Tethysetta* sp., M8 14.30, 020112, 200x.
- Fig. 35 - *Ristola altissima major* Baumgartner & De Wever, M8 38.40, 030216, 150x.
- Fig. 36 - *Ristola altissima altissima* (Rüst), M8 10.90, 031023, 150x.

PLATE 4

Radiolarians from Unit 4 of Mt. Mangart section. For each illustration the sample number, SEM negative number, and magnification are indicated.

- Figs. 1-2 - *Hsuum rutogense* Yang & Wang. Fig. 1) M8 21.90, 030822; Fig. 2) M8 33.30, 030316; 200x.
- Fig. 3 - *Archaeodictyomitra? amabilis* Aita, M8 33.30, 030321, 200x.
- Figs. 4-5 - *Parahsuum carpathicum* Widz & De Wever, M8 10.90. Fig. 4) 031007; Fig. 5) 031010; 200x.
- Fig. 6 - *Archaeodictyomitra apiarium* (Rüst), M8 14.30, 020117, 200x.
- Figs. 7-8 - *Archaeodictyomitra minoensis* (Mizutani). Fig. 7) M8 14.30, 020102; Fig. 8) M8 10.20, 031003, 200x.

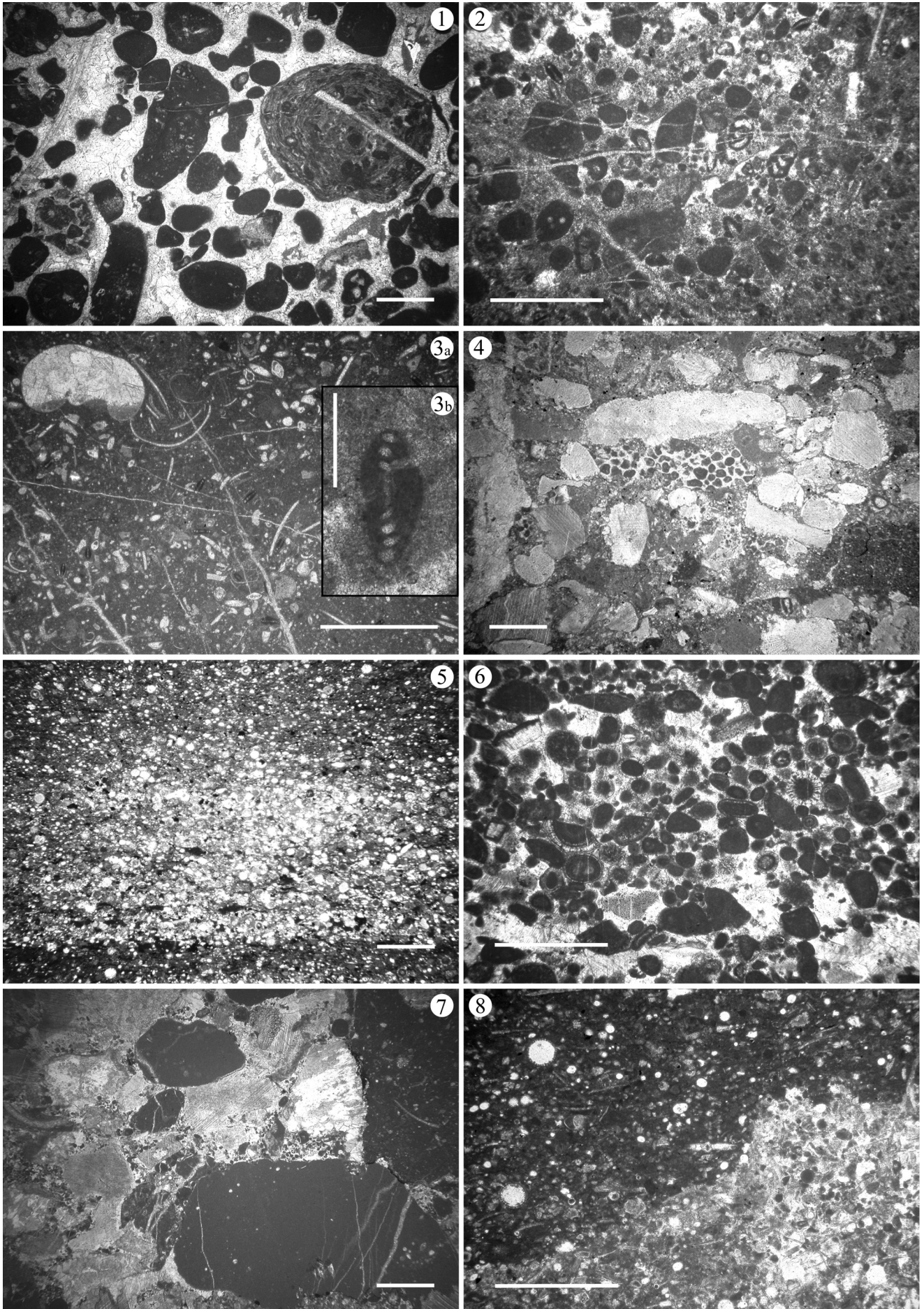


PLATE 1

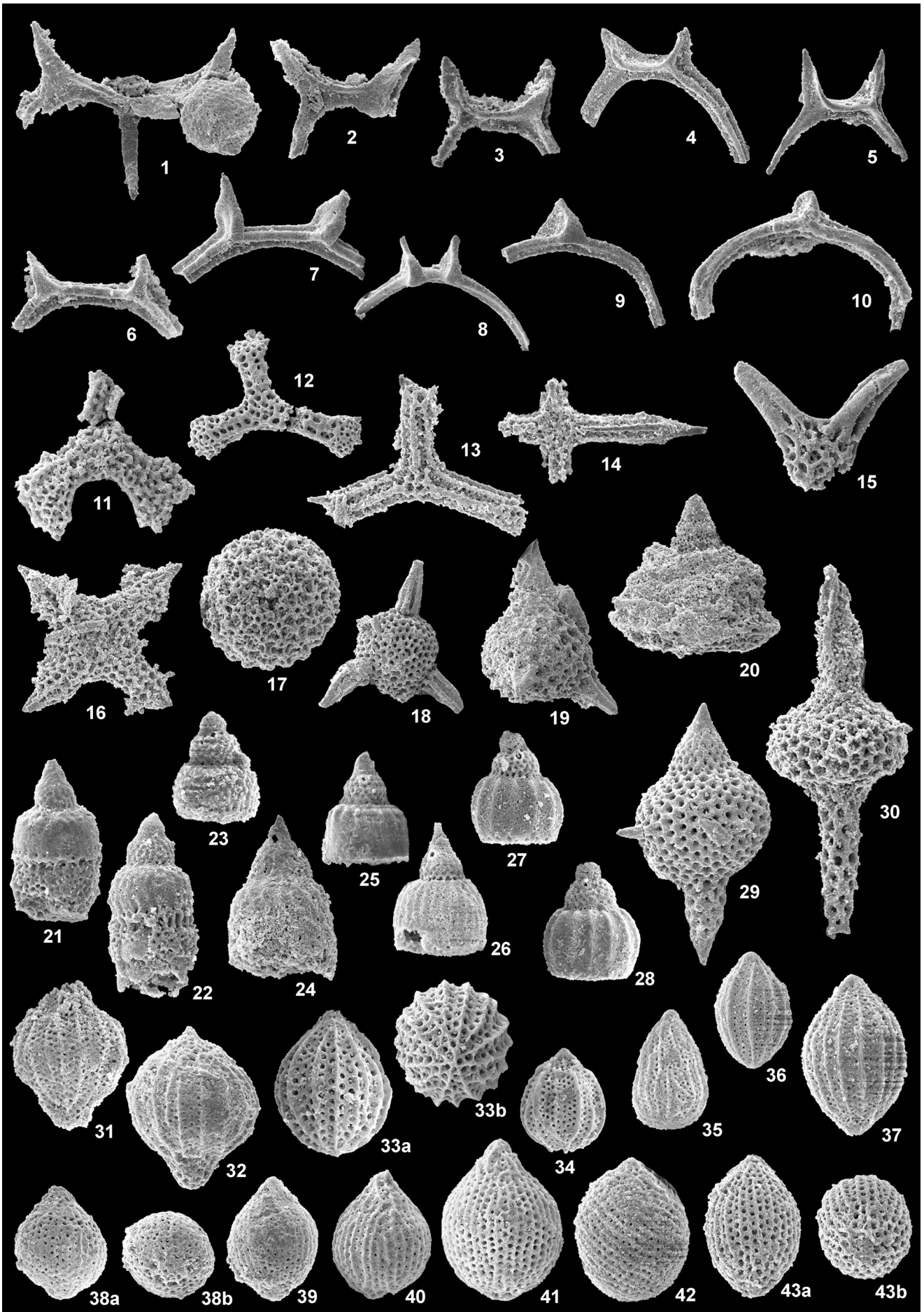


PLATE 2

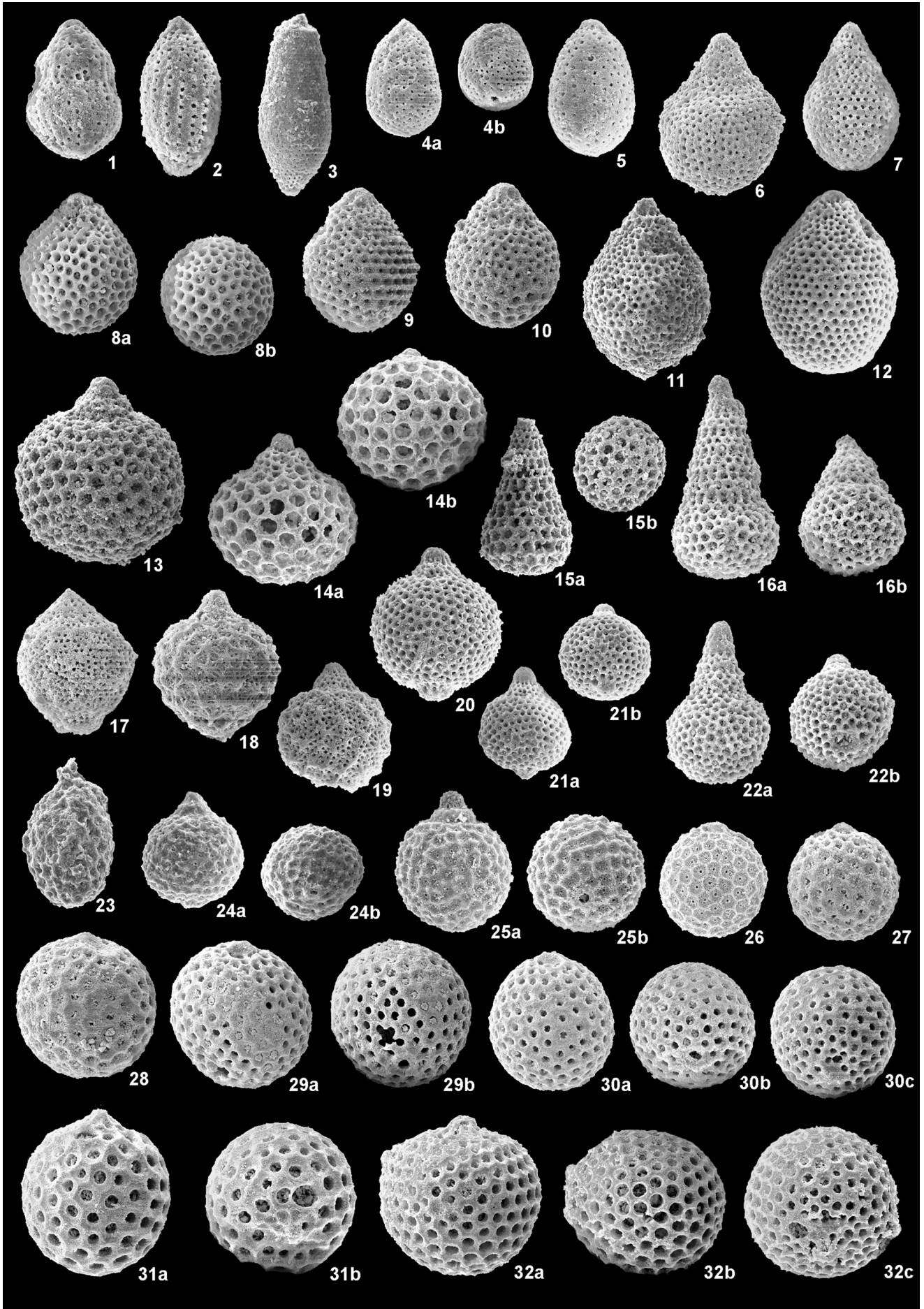


PLATE 3

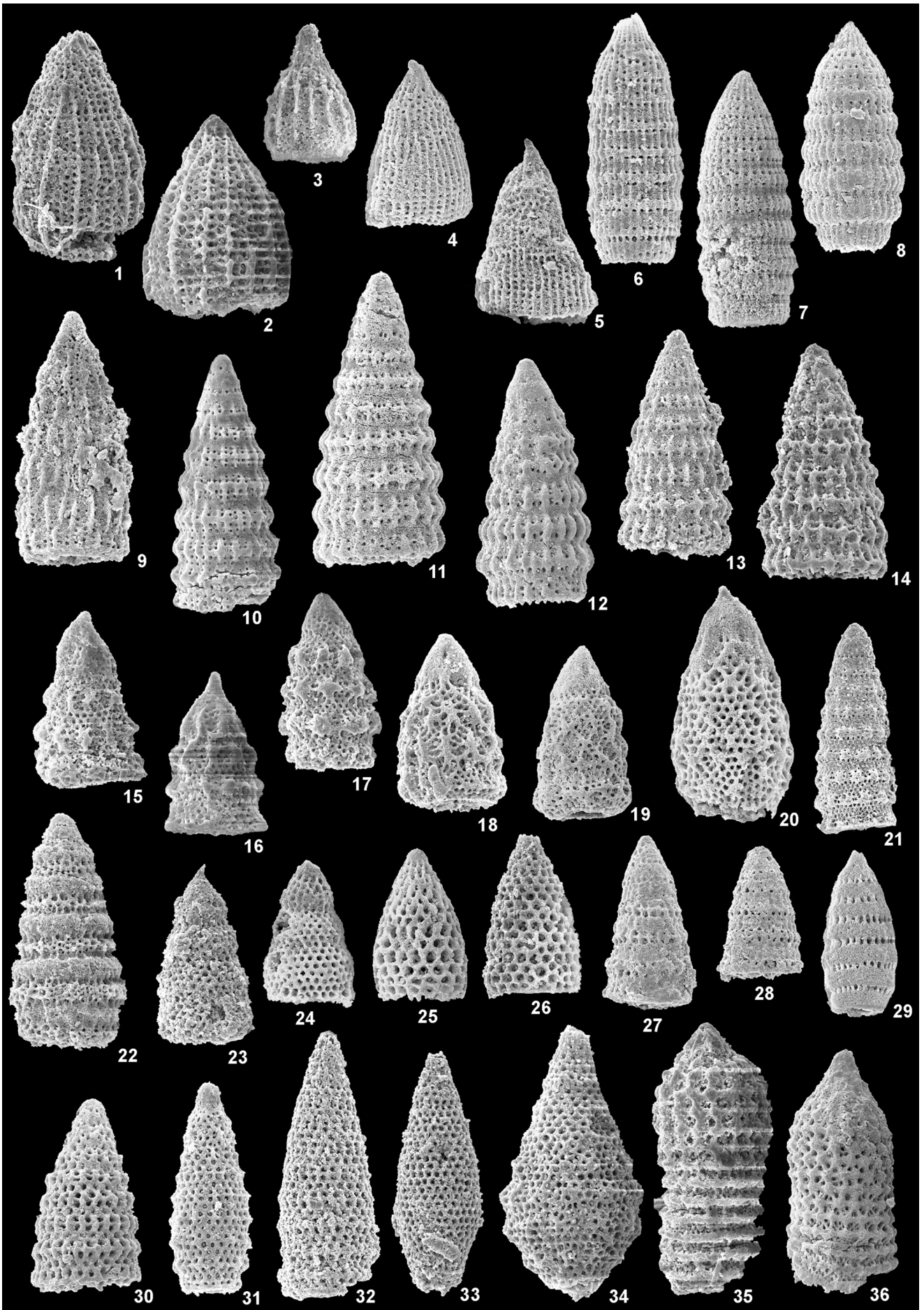


PLATE 4

Gongylothorax ponticus Bragin & Tekin, 2002

Pl. 3, figs 4a-b, 5

2002 *Gongylothorax ponticus* Bragin et al., p. 624, Fig. 7.15-17.**Gongylothorax sp. A**

Pl. 3, figs 27, 28, 29a-b, 30a-c

Remarks. This species is closely related to *Gongylothorax favosus* Dumitrica, from which it differs in having larger pores. The ridges around hexagonal areas are more elevated in relief. *Gongylothorax* sp. A was found only in sample M8 6.80.

Hexasaturnalis suboblongus ssp. A

Pl. 2, fig. 3-5

1995a *Acanthocircus suboblongus suboblongus* (Yao) - Baumgartner et al., p. 68, pl. 3088, fig. 1, not figs 2-4.

Remarks. This subspecies has the external blades of the ring fused on one spine and separated on the other spine. In *Hexasaturnalis suboblongus suboblongus* (Yao) the blades on both spines are separated, whereas in *Hexasaturnalis suboblongus minor* (Baumgartner) both spines have fused blades. In Baumgartner et al. (1995a) *Hexasaturnalis suboblongus* ssp. A was included in *Hexasaturnalis suboblongus suboblongus*. According to Dumitrica (pers. comm. 2003) *Hexasaturnalis suboblongus* ssp. A first appears in the Bathonian.

Hsuum rutogense Yang & Wang, 1990

Pl. 4, figs 1-2

1990 *Hsuum rutogense* Yang & Wang, p. 207, pl. 3, figs 2, 4, 10.
1990 *Hsuum* cf. *rutogense* Yang & Wang, p. 208, pl. 4, fig. 15.

Levileugeo ordinarius Yang & Wang, 1990

Pl. 2, fig. 17

1990 *Levileugeo ordinarius* Yang & Wang, p. 203, pl. 1, figs. 2, 14; pl. 2, fig. 1.

Loopus doliolum Dumitrica, 1997

Pl. 4, fig. 29

1997 *Loopus doliolum* Dumitrica et al., p. 30, pl. 5, figs. 3, 5, 14.**Parahsuum carpathicum** Widz & De Wever, 1993

Pl. 4, figs 4-5

1993 *Parahsuum carpathicum* Widz & De Wever, p. 85, pl. 1, figs 14-16.

Podobursa rosea Hull, 1997

Pl. 2, fig. 30

1997 *Podobursa rosea* Hull, p. 102, pl. 42, figs. 2, 3, 15, 17, 20.**Podobursa triacantha** (Fischli, 1916)

Pl. 2, fig. 29

1997 *Podobursa triacantha* - Hull, p. 106, pl. 41, figs. 1-3, 5, 15, 16, 19 (and synonymy therein).

Protunuma ? aff. lanosus Ozvoldova, 1996

Pl. 2, fig. 35

aff. 1996? *Protunuma lanosus* Sykora & Ozvoldova, p. 23, pl. 2, fig. 13, pl. 3, figs. 1-6.

Remarks. This morphotype differs from the type material by having a more elongated test.

Stichomitra? annibill Kocher, 1981

Pl. 4, fig. 24

1981 *Stichomitra annibill* Kocher, p. 96, pl. 16, figs. 24-26.
1997 *Stichomitra* (?) *matsuokai* Hull, p. 164, pl. 49, figs. 2, 3, 13, 14, 19, 20.

Stichomitra ? tairai Aita, 1987

Pl. 4, fig. 23

1987 *Stichomitra* (?) *tairai* Aita, p. 72, pl. 3, figs. 7a-b, 8a-b, 9; pl. 10, figs. 3-4.

Striatojaponocapsa? matsuokai (Sashida, 1999)

Pl. 2, figs 43 a-b

1999 *Tricolocapsa matsuokai* Sashida et al., p. 566, pl. 1, figs. 4-5.**Theocapsomma medvednicensis** Gorican, 1999

Pl. 3, fig. 1

1999 *Theocapsomma medvednicensis* Halamic et al., p. 37, pl. 1, figs. 12a-b, 13, 14a-b, 15-16.

Unuma darnoensis Kozur, 1991

Pl. 2, fig. 32

1991 *Unuma darnoensis* Kozur, pl. 2, fig. 2.
1994 *Unuma darnoensis* - Gorican, p. 95, pl. 10, figs. 7-8, 9a-b.

Unuma gordus Hull, 1997

Pl. 2, fig. 34

- 1995a *Unuma* sp. A - Baumgartner et al., p. 624, pl. 3309, figs 1-4.
 1997 *Unuma gorda* Hull p., 172, pl. 43, figs 9, 11, 12.

Williriedellum yahazuense (Aita, 1987)

Pl. 3, fig. 19

1987 *Sethocapsa yahazuensis* Aita, p. 73, pl. 2, figs 88a-b, 9a-b; pl. 9, figs 16-17.

Williriedellum yaoi (Kozur, 1984)

Pl. 3, figs 24 a-b, 25 a-b

1984 *Praezhamoidellum yaoi* Kozur, p. 53, pl. 3, figs 3a-b.

Xitus skenderbegi (Chiari, Marcucci & Prella, 2002)

Pl. 4, figs 15, 16

2002 *Neorelumbra skenderbegi* Chiari et al., 68, pl. 1, figs 14-21.

Depositional history of Mt. Mangart succession

The Mt. Mangart area underwent tectonic extension related to the formation of the southern Tethyan continental margin that started in the latest Triassic and continued into the Jurassic (Bertotti et al. 1993). The Mt. Mangart succession allows us to observe the transition from shallow-water carbonate platform to deeper-water basin, to reconstruct a depositional history of the basin-margin depositional system, and to discuss the main mechanisms controlling the sedimentation on a Jurassic southern Tethyan margin. For major facies changes and second-order transgressive-regressive cycles, discussed in this chapter see Fig. 5.

Lower Jurassic shallow water sedimentation and demise of the carbonate platform.

The limestones of Unit 1 formed as a sand belt in the marginal sector of a shallow-water platform recording the Early Jurassic continuation of shallow-water sedimentation since the latest Triassic. The finer-grained peloidal wackestones/packstones in the upper part of the Unit 1 were formed in a hydrodynamically quieter environment. They contain open marine elements (*Lenticulina*), thus indicating deepening of the environment. Because limestones of Unit 1 are the last evidence of shallow-water deposition, that was never fully reestablished, we interpret this deepening as being controlled predominately by increased rates of tectonic subsidence in the early Pliensbachian related to the development of the southern Tethyan continental margin. At that time, a shallow-water platform was dissected into blocks with different subsidence rates. The intercalated peloidal wackestone/packstones are thus interpreted as markers

of incipient drowning. Continuously increasing tectonic subsidence rates probably coupled with carbonate productivity decrease due to the eutrophication (cf. Dromart et al. 1996; Mallarino et al. 2002; Morettini et al. 2002) caused complete drowning of the Mangart block in the Pliensbachian. As a consequence, distal shelf limestones with sponge spicules and juvenile ammonites of Unit 2 began to accumulate.

In the upper part of the Unit 2, breccias and calcarenites composed mainly of echinoderm fragments and clasts of underlying lithologies are present. We interpret that their formation is related to a synsedimentary extensional tectonic pulse in the Pliensbachian that produced an unstable slope, uncovered older rocks and enabled erosion. The facies change from distal shelf limestones to echinoderm breccias and calcarenites is similar to the change observed in the transition from the Inici M3 Member to the Calcari a Crinoidi Formation at Monte Kumeta in western Sicily (Di Stefano et al. 2002). This change is similarly interpreted as a consequence of further down-faulting and relative sea-level rise (Di Stefano et al. 2002).

The pelagic wackestone and packstone with sponge spicules, radiolarians, and ferromanganese nodules overlying breccias and calcarenites suggest extremely reduced sedimentation rates that reached a minimum with the formation of a 25 cm thick Fe-Mn hardground. We interpret this slowing of the sedimentation rates and formation of the Fe-Mn nodules and crusts as a result of the late Pliensbachian widespread Tethyan regression (R5 in Graciansky et al. 1998) that induced strong bottom currents sweeping off the sea floor and thus prevented high sediment accumulation (Martire 1992, 1996).

For the Trento Plateau, which was a part of the same rifted margin, a depositional depth of a few hundred meters was assumed for the uppermost Lower Jurassic to lower Middle Jurassic ferromanganese hardground that marks an unconformity surface (Winterer & Bosellini 1981). However, other authors (Zempolich 1993; Clari & Masetti 2002) proposed shallower water depths and suggested subaerial exposure (Zempolich 1993) in order to explain the unconformity in the Trento Plateau. On the contrary, the Fe-Mn nodules at Mt. Mangart occur within a pelagic limestone with sponge spicules and radiolarians, and are overlain by black shales and radiolarian-bearing limestones. Therefore they clearly show a slowing of sedimentation rates within marine environment, probably some hundreds of meters deep (cf. Winterer & Bosellini 1981; Martire 1992).

Toarcian anoxic basin

The limestones in the lower part of the Unit 3 represent the upward continuation of open marine sedimentation and indicate that sedimentation rates in-

creased most probably because of weakening of bottom currents due to the early Toarcian transgression (T6 in Graciansky et al. 1998) and an important input of terrigenous clastics. Organic-rich shales with intercalated siliceous limestones represent anoxic sediments deposited during the early Toarcian Oceanic Anoxic Event, also recognized in other parts of the Mediterranean including the Southern Alps (Jenkyns 1985, 1988; Jenkyns et al. 1985; Jenkyns & Clayton 1986; Baudin et al. 1990). The Mt. Mangart area at that time acted as an anoxic basin trapping the fine-grained sediments. According to Jenkyns et al. (1991) these basins were located within the oxygen minimum zone. Intercalated beds of siliceous limestone were deposited by fine-grained turbidites. An early to middle Toarcian transgressive-regressive cycle (T6/R6 in Graciansky et al. 1998) is recorded within Unit 3 with maximum transgression represented by the most abundant intercalations of siliceous limestones within shales in the lower part of the unit (Fig. 5). At the same level, a peak in abundance of the radiolarian family Pantanelliidae was recorded, that may indicate the maximum development of eutrophic conditions (Gorican et al. 2003).

Bajocian rapid subsidence followed by deep basinal sedimentation

In the Bajocian a major reorganization in sedimentation style of the investigated area occurred. The Mt. Mangart succession at that time became a part of a deeper basin with sedimentation of cherts and siliceous limestones with radiolarians, and started to receive carbonate resediments from the adjacent Friuli (Dinaric) Carbonate Platform. We interpret this reorganization as a consequence of accelerated subsidence that occurred prior to the late Bajocian. Increased subsidence rates in the Bajocian are also recognized westward in the Belluno Basin and on the Trento Plateau (Winterer & Bosellini 1981; Martire 1992, 1996; Winterer 1998). A long stratigraphic gap (at least from late Toarcian to early Bajocian) separating Unit 3 from Unit 4 is here interpreted primarily as a result of extremely slow sedimentation rates due to sediment bypass as evidenced by borings at the top of Unit 3. This discontinuity surface is correlative with the Mid-Cimmerian unconformity recorded in most of the European basin margins and structural intrabasinal highs (Jacquin & Graciansky 1998; Jacquin et al. 1998).

The fine-grained sediments overlying basal breccias of the Unit 4 are assigned to the UAZ 5 (latest Bajocian-early Bathonian) radiolarian zone of Baumgartner et al. (1995c). The same radiolarian zone was reported in radiolarian cherts overlying the oldest Jurassic ophiolites in the Dinarides – Hellenides, well documented e.g. in the Mirdita Zone of Albania (Prela et al. 2000). Moreover, in the Alpine Tethys, the oceanic

spreading also started during the Bajocian (review in Bill et al. 2001). We can thus deduce that the rapid subsidence of the continental margin in the Bajocian was a response to oceanic opening in the western Tethys.

In general, the Middle and Upper Jurassic deposits of the Mt. Mangart succession (Unit 4) are dominated by siliceous and carbonate background sediments (cherty limestones, cherts and siliceous mudstones) and abundant platform-derived carbonates that occur as coarse debris-flow deposits, and coarse to fine-grained turbidites.

Background sediments contain plankton (radiolarians), open marine benthos (sponge spicules, filaments) and also variable amounts of carbonate mud. The carbonate admixture in these beds can be either of pelagic or platform origin. However, since the planktic carbonate producers were scarce in the Middle Jurassic we assume that at least part of the carbonate mud is allochthonous and exported off-platform (cf. Baumgartner 1987; Cobianchi & Picotti 2001; Bartolini et al. 2002; Mattioli & Pittet 2002; Pittet & Mattioli 2002). The background sedimentation shows prominent increase in the clay admixture in the upper part of the Unit 4, which is the highest in the 2.5 m thick clay-rich package dated as middle-late Oxfordian. We interpret this increased clay content as a consequence of a warm and humid climate in the middle-late Oxfordian that enhanced weathering and therefore increased clay input to the basins (cf. Weissert & Mohr 1996).

The variable amount of calcareous gravity-flow deposits interstratified within pelagic background deposits allows the recognition of sea-level changes. Basal breccias and calcarenites of M1 member contain reworked older lithoclasts and many highly evolved glauconitic grains. Some glauconitic grains still have preserved fractures on grain surface thus indicating that they were transported over relatively short distances. Glauconitic grains thus represent resedimented-parautochthonous glauconitic grains (cf. Amorosi 1997) and indicate long sediment starvation in the provenance area (Odin & Fullagar 1988; Amorosi 1995, 1997). Parautochthonous glaucony commonly occurs in transgressive system tracts (Amorosi 1997; Harris & Whiting 2000; Cattaneo & Steel 2003). We therefore interpret basal breccias and calcarenites in the lower part of the Member M1 of the Unit 4 as transgressive deposits. On the other hand, the reworked lithoclasts document an important submarine erosion event cutting into the substratum down to Unit 2, which was probably exposed due to normal faulting. It should be mentioned that other neighboring sections of the same structural unit show a several meters thick turbidite succession below the correlative breccias. The formation of breccias thus cannot be simply a response to the major subsidence pulse in the Bajocian. Breccias and calcarenites could

be related to the oversteepening and back-steeping of the basin margin as transgression proceeds (cf. Emery & Myers 1996) or they could mark another extensional tectonic pulse creating slope instability due to normal faulting.

Homogenous wackestone with radiolarians of M1 may correspond to a flooding of the adjacent carbonate platform (T7/R7 in Jacquin et al. 1998) and thus maximum off-shore transport of lagoonal mud (cf. Schlager et al. 1994). The lowermost part of the M3 member is marked by amalgamated breccia beds abruptly overlain by fine-grained calcarenites and thus indicate sediment by-pass. Breccia beds bounded by erosional surfaces are considered to be the most diagnostic facies of the basal portions of many erosional and mixed channel-fill sequences (Mutti 1992). They represent the most proximal facies association of Unit 4 and are correlative with the late Bathonian lowstand (R7/T8 in Jacquin et al. 1998). General thinning and fining upward trend from upper Bathonian (top of M3) to Callovian-Oxfordian (lower and middle part of the M4) and then coarsening-upward trend in the Oxfordian (see Fig. 5) corresponds to the second-order transgressive-regressive cycle 8 of Jacquin et al. (1998). Of special interest are breccia bed and coarse-grained calcarenites in the upper part of the Unit 4. They contain large eroded clasts of underlying lithologies and also detritic grains of bytownite-anorthite feldspars and represent the most proximal facies in the uppermost part of the Unit 4. Occurrence of the breccia coincides approximately with the onset of a compressive regime in the internal domains of the Dinarides (Chanell et al. 1979, see also discussion in Goričan 1994) and Hellenides (Baumgartner 1985). In the most external domains of the Dinarides this event resulted in major uplift and emersion of the Friuli (Dinaric) Platform as evidenced by widespread bauxites overlain by Tithonian limestones with *Clypeina jurassica* (Favre) (Dozet 1994; Dozet et al. 1996). Therefore we interpret the breccias in the upper part of the Unit 4 to be related to convergent plate movements in the Dinaric Tethys, that caused normal faulting and differential subsidence in pre-existing basins located in external domains. The origin and provenance of the detritic grains of bytownite-anorthite feldspars is, however, still enigmatic and difficult to interpret from the single occurrence so far recorded.

Carbonate resediments of Unit 4 also record changes in sediment production on the adjacent Friuli Carbonate Platform. Oolitic megabeds of M2 correspond to a maximum of oolitic production on the platform in the Bathonian. From M2 upward the carbonate resediments show increase in skeletal and concomitant decrease in ooidal content, resulting in the beds composed exclusively of echinoderm fragments in the uppermost part of the Unit 4, as already observed by

Bosellini et al. (1981) in the coeval succession of the Belluno Basin.

Middle to Upper Jurassic resedimented limestones are characteristic of many Tethyan basins located close to carbonate platforms, e.g. Belluno Basin in the Southern Alps (Bosellini et al. 1981; Winterer & Bosellini 1981; Clari & Masetti 2002), Sabina Basin of Umbria-Marche Apennines (Bartolini et al. 1996, 1999; Santantonio & Muraro 2002), Slovenian Basin (Cousin 1981) and Budva Basin (Goričan 1994) in the Dinarides.

Carbonate pelagic sedimentation

At the lower/upper Tithonian boundary, the siliceous background sedimentation (cherts and cherty limestones of Unit 4) was replaced by carbonate background sedimentation (nodular limestones with chert layers of Unit 5). Abrupt facies change to the calcareous Biancone Formation is also observed in the Slovenian Basin (Cousin 1981; Buser 1986, 1987) and further south in the Dinarides (e.g. Goričan 1994). In the Southern Alps, an overall gradual increase in carbonate pelagic sedimentation is observed from the Oxfordian to the lower Cretaceous (Weissert 1979; Winterer & Bosellini 1981; Baumgartner 1987; Baumgartner et al. 1995b; Bartolini et al. 1999).

Correlation with Belluno Basin and Slovenian Basin

The Mt. Mangart area is located in the region where the Southern Alps overlap with the Dinarides. It lies between the Belluno Basin and the Slovenian Basin (see Fig. 2) and represents a possible paleogeographic connection between them. We therefore correlate the Mt. Mangart succession with the successions of the Belluno and the Slovenian Basin (Fig. 7).

Correlation with the Belluno Basin

At Mt. Mangart the lower Lower Jurassic shallow water deposits of Unit 1 are overlain by Pliensbachian deeper-water limestones of Unit 2. This mirrors the western part of the Belluno Basin where lower Lower Jurassic Calcarei Grigi are overlain by a cherty limestone of the Soverzene Formation (Masetti & Bianchin 1987) but differs from the central part of the Belluno Basin where the Soverzene Formation ranges down to the Hettangian.

Unit 3 is correlative to the Toarcian black shales, a member of the Igne Formation of the Belluno Basin (Masetti & Bianchin 1987). The early Toarcian Oceanic Anoxic Event was recorded in both areas. However, the Igne Formation is much thicker, in general more calcareous, and also contains middle Toarcian to lower-?upper Bajocian deposits: limestones and dolomitic limestones with interbeds of marls and dolostones with

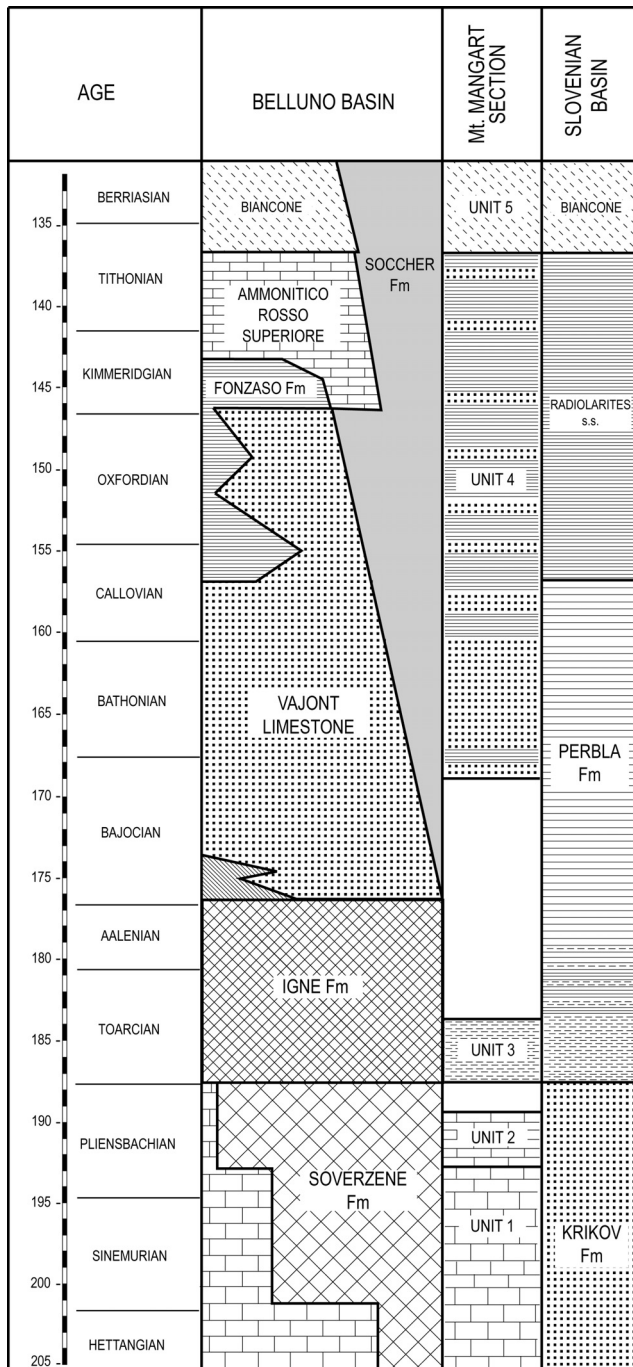


Fig. 7 - Correlation of Mt. Mangart section with the successions of the Belluno Basin and Slovenian Basin (Belluno Basin after Baumgartner et al. 1995b, Slovenian Basin compiled after Cousin 1981 and Buser 1987).

chert layers and nodules (Bellanca et al. 1999; Clari & Masetti 2002), while these deposits are completely missing at Mt. Mangart.

Resedimented limestones of M1, M2, and M3 of Unit 4 are time and facies equivalents of the Vajont Limestone (Bosellini et al. 1981). The age of the Vajont Limestone has been a matter of debate. On the basis of calcareous nannoplankton Zempolich and Erba (1999) proposed Aalenian to late Bajocian age, but Clari and

Masetti (2002) assigned the Vajont Limestone to the late Bajocian to Bathonian. Our radiolarian data are consistent with the dates of Clari and Masetti (2002).

The M4 member of Unit 4 is correlative to the Callovian to lower Kimmeridgian Fonzaso Formation and overlying Ammonitico Rosso Superiore. Unit 5 is equivalent to the Biancone Formation of the Belluno Basin (e.g. Baumgartner et al. 1995b; Clari & Masetti 2002).

The Mt. Mangart succession correlates well with the successions of the Belluno Basin. However, the re-sedimented limestones of the Vajont Formation are much thicker in the Belluno Basin (800 to 1000 m in most proximal sectors) than coeval M1 to M3 members of Unit 4 of Mt. Mangart (42 m). This can be explained by paleobathymetry. The Mangart subsided block was located closer to the Friuli Platform and was topographically higher, which is also suggested by its relatively late initial subsidence, conspicuous hiatuses and obvious sediment bypass within Unit 4. On the other hand, in the Slovenian Basin the oolitic resediments are also very thin (25 m in most proximal areas – see below). Oolite deposition on the platform was strongly controlled by surface currents (Bosellini et al. 1981). A windward position of north-eastern margin of the Friuli Platform facing the Slovenian Basin is thus probable, so that most of the ooids were transported in south-western direction towards the Belluno Basin (Wright & Burchette 1996, p. 368).

Another important observation is that at Mt. Mangart, a thin layer of coarse-grained breccia composed of reworked basinal rocks and feldspars was found at the top of Unit 4. This layer roughly correlates with the Fonzaso Formation/Ammonitico Rosso boundary. A similar breccia is not known in the Belluno Basin.

Correlation with the Slovenian Basin

Units 1 and 2 of the Mt. Mangart succession are time equivalent to the Lower Jurassic Krikov Formation (Cousin 1970, 1981; Buser 1986, 1987), characterised by deeper-water resedimented limestones with cherts similar to the Soverzene Formation of the Belluno Basin. Unit 3 is correlative with lower part of the Perbla Formation (Cousin 1970, 1981; Buser 1986, 1987) that consists primarily of shales. Unit 4 correlates with middle and upper part of the Perbla Formation (calcareous shales and siliceous limestones) and with radiolarites (black, green and red cherts). Resedimented limestones are locally intercalated in the Perbla Formation and in the radiolarites but are much thinner than those of Mt. Mangart. Coarse to medium-grained resedimented deposits occur only in the most proximal settings whereas distal parts of the Slovenian Basin are characterized only by fine-grained calcareous turbidites.

The Unit 5 of the Mt. Mangart succession is equivalent of the Biancone Limestone in the Slovenian Basin.

The Mt. Mangart succession and the preserved Slovenian Basin successions are generally similar. However, there are important differences. The Slovenian Basin was a deeper basin at the beginning of the Jurassic while Mt. Mangart was still a shallow-water carbonate platform. The transition from the Krikov Formation to the Perbla Formation in the Slovenian Basin is continuous, whereas at Mt. Mangart, the correlative U2/U3 boundary is discontinuous (Fe-Mn hardground). An important stratigraphic gap is also recorded between U3 and U4 at Mt. Mangart, whereas the Slovenian Basin was characterized by a continuous sedimentation at that time. The preserved proximal successions of the Slovenian Basin contain less oolitic resediments (up to 25m) (Cousin 1981; Rozic 2003a,b). On the basis of these differences we conclude that the preserved successions of the Slovenian Basin were deeper and located more distally from the Friuli (Dinaric) Carbonate Platform than Mt. Mangart.

Conclusions

The Jurassic Mt. Mangart succession belongs to a subsided platform margin that contains a record of rifting history, platform drowning and subsequent basinal deposition. The succession correlates with regional tectonics, eustatic sea-level changes and major paleoceanographic changes as follows:

1. Shallow water sedimentation at Mt. Mangart lasted until the early Pliensbachian (Unit 1), when the carbonate platform was drowned due to the increased tectonic subsidence probably coupled with carbonate production decrease. Consequently, distal-shelf deposits started to accumulate. Further downfaulting continued into the late Pliensbachian as evidenced by breccias and calcarenites in the upper part of Unit 2.

2. The Fe-Mn hardground separating Unit 2 and Unit 3 has been interpreted as the local record of the Pliensbachian/Toarcian lowstand.

3. The black and brown shales, capped by an intensively bored limestone (Unit 3) record the Toarcian transgressive/regressive cycle.

4. The stratigraphic gap spanning the late Toarcian to early Bajocian corresponds to the Mid-Cimmerian unconformity.

5. The accelerated subsidence prior to the late Bajocian caused further deepening. Mt. Mangart became a part of a deeper basin with siliceous background se-

dimentation and important carbonate input from the adjacent Friuli Carbonate Platform.

6. Coarse-grained breccias capped by fine-grained calcarenites at the base of the M3 member are interpreted as the most proximal facies association of Unit 4 and probably reflect late Bathonian regression.

7. The subsequent maximum transgression is placed in the Callovian – Oxfordian siliceous sediments of Unit 4, where the most distal calcareous turbidites are intercalated.

8. An increased input of clayey material occurred in the middle-late Oxfordian and was related to a warming and more humid climate.

9. The formation of the overlying coarse-grained breccia with basinal lithoclasts and feldspars could be related to tectonic movements during the first stages of compression in more internal Dinaric domains.

10. In the Tithonian, the succession shows a change from siliceous to carbonate pelagic sedimentation that is a regional characteristic of basinal successions in the Southern Alps and Dinarides.

Comparison with the Belluno Basin and Slovenian Basin shows that Mt. Mangart is similar to the sections in the marginal part of the Belluno Basin. In the early Early Jurassic the Slovenian Basin and most of the Belluno Basin were already deep-water basins while the Mt. Mangart area was a carbonate platform that was drowned not earlier than in the early Pliensbachian. Mt. Mangart became a part of a deeper basin in the late Bajocian. The preserved Middle to Upper Jurassic successions of the Belluno and the Slovenian Basin were deposited in deeper basinal settings located more distally from the Friuli (Dinaric) Platform than the Mt. Mangart succession.

Considering the present day facies distribution (Fig. 2), these facts could indicate that the Belluno Basin and the Slovenian Basin were not continuous but were wedge-shaped and, at least during early Early Jurassic, disconnected by a topographic high preserved in the Mt. Mangart succession. However, detailed stratigraphic research, as well as structural analysis of Jurassic rocks in the western Julian Alps, are needed to obtain a reliable, more extensive paleogeographic reconstruction of this region in the Jurassic.

Acknowledgements. This study was supported financially by the Ministry of Education, Science and Sport, Republic of Slovenia (project number P0-0521-0618). We thank Kata Cvetko-Baric for preparation of thin sections, and Petra Meglic and Nevenka Sorli for preparation of radiolarian residues. We are much obliged to Adrijan Kosir as well as to the reviewers Luca Martire and Daniele Masetti for thorough review of the manuscript. Glenn Jaecks is gratefully acknowledged for English corrections of the final text.

REFERENCES

- Aita Y. (1987) - Middle Jurassic to Lower Cretaceous Radiolarian Biostratigraphy of Shikoku with Reference to Selected Sections in Lombardy Basin and Sicily. *Tohoku Univ., Sci. Rep.*, 2nd ser. (Geol.) 58/1: 1-91, pls. 1-14, Sendai.
- Amorosi A. (1995) - Glaucony and Sequence Stratigraphy: A Conceptual Framework of Distribution in Siliciclastic Sequences. *J. Sedim. Research*, B65/4: 419-425, Tulsa.
- Amorosi A. (1997) - Detecting compositional, spatial and temporal attributes of glaucony: a tool for provenance research. *Sedim. Geology*, 109: 135-153, Amsterdam.
- Aubouin J., Bosellini A. & Cousin M. (1965) - Sur la paléogéographie de la Vénétie au Jurassique. *Mem. Geopal. Univ.*, 1: 147:158, Ferrara.
- Bartolini A., Baumgartner P.O. & Hunziker J.C. (1996) - Middle and Late Jurassic carbon stable-isotope stratigraphy and radiolarite sedimentation of the Umbria-Marche Basin (Central Italy). *Eclogae geol. Helv.*, 89: 831-879, Basel.
- Bartolini A., Baumgartner P.O. & Guex J. (1999) - Middle and Late Jurassic radiolarian palaeoecology versus carbon-isotope stratigraphy. *Palaeogeogr., Palaeoclim., Palaeoecol.*, 145: 43-60, Amsterdam.
- Bartolini A., Pittet B., Mattioli E. & Hunziker J.C. (2002) - Shallow-platform palaeoenvironmental conditions recorded in deep-shelf sediments: C and O stable isotopes in Upper Jurassic sections of southern Germany (Oxfordian-Kimmeridgian). *Sedim. Geology*, 160: 107-130, Amsterdam.
- Baudin F., Herbin J.P., Bassoulet J.P., Dercourt J., Lanchkar G., Manivit H. & Renard M. (1990) - Distribution of Organic Matter during the Toarcian in the Mediterranean Tethys and Middle East. In: Huc A.Y. (ed.) - Deposition of Organic Facies. *AAPG Studies in Geology*, 30: 73-91, Tulsa.
- Baumgartner P.O. (1985) - Jurassic Sedimentary Evolution and Nappe Emplacement in the Argolis Peninsula (Peloponnesus, Greece). *Denksch. Schweiz. Naturf. Gesell.*, 99: 111 pp., Basel.
- Baumgartner P.O. (1987) - Age and genesis of Tethyan Jurassic Radiolarites. *Eclogae geol. Helv.*, 80/3: 831-879, Basel.
- Baumgartner P. O., O'Dogherty L., Gorican S., Dumitrica-Jud R., Dumitrica P., Pillecuit A., Urquhart E., Matsuoka A. & Danelian T. (1995a) - Radiolarian catalogue and systematics of Middle Jurassic to Early Cretaceous Tethyan genera and species. In: Baumgartner P. O., O'Dogherty L., Gorican S., Urquhart E., Pillecuit A. & De Wever P. (eds.) - Middle Jurassic to Lower Cretaceous Radiolaria of Tethys: Occurrences, Systematics, Biochronology. *Mém. Géologie*, 23: 37-688, Lausanne.
- Baumgartner P.O., Martire L., Gorican S., O'Dogherty L., Erba E. & Pillecuit A. (1995b) - New Middle and Upper Jurassic radiolarian assemblages co-occurring with ammonites and nannofossils from the Southern Alps (Northern Italy). In: Baumgartner P. O., O'Dogherty L., Gorican S., Urquhart E., Pillecuit A. & De Wever P. (eds.) - Middle Jurassic to Lower Cretaceous Radiolaria of Tethys: Occurrences, Systematics, Biochronology. *Mém. Géologie*, 23: 737-750, Lausanne.
- Baumgartner P. O., Bartolini A., Carter E. S., Conti M., Cortese G., Danelian T., De Wever P., Dumitrica P., Dumitrica-Jud R., Gorican S., Guex J., Hull D. M., Kito N., Marcucci M., Matsuoka A., Murchey B., O'Dogherty L., Savary J., Vishnevskaya V., Widz, D. & Yao A. (1995c) - Middle Jurassic to Early Cretaceous radiolarian biochronology of Tethys based on Unitary Associations. In: Baumgartner P. O., O'Dogherty L., Gorican S., Urquhart E., Pillecuit A. & De Wever P. (eds.) - Middle Jurassic to Lower Cretaceous Radiolaria of Tethys: Occurrences, Systematics, Biochronology. *Mém. Géologie*, 23: 1013-1038, Lausanne.
- Bellanca A., Masetti D., Neri R. & Venezia F. (1999) - Geochemical and sedimentological evidence of productivity cycles recorded in Toarcian Black Shales from the Belluno Basin, Southern Alps, Northern Italy. *J. Sedim. Research*, 69/2: 466-476, Tulsa.
- Bernoulli D., Bertotti G. & Froitzheim N. (1990) - Mesozoic faults and associated sediments in the Austroalpine-South Alpine continental margin. *Mem. Soc. Geol. Ital.*, 45: 25-38, Roma.
- Bertotti G. (1991) - Early Mesozoic extension and Alpine tectonics in the Western Southern Alps. The geology of the area between Lugano and Menaggio (Lombardy, northern Italy). *Mem. Sci. Geol.*, 43: 17-123, Padova.
- Bertotti G., Picotti V., Bernoulli D. & Castellarin A. (1993) - From rifting to drifting: tectonic evolution of the South-Alpine upper crust from the Triassic to the Early Cretaceous. *Sedim. Geology*, 86: 53-76, Amsterdam.
- Bill M., O'Dogherty L., Guex J., Baumgartner P.O. & Masson H. (2001) - Radiolarite ages in Alpine-Mediterranean ophiolites: Constraints on the oceanic spreading and the Tethys-Atlantic connection. *GSA Bulletin*, 113/1: 129-143, Boulder.
- Bosellini A., Masetti D. & Sarti M. (1981) - A Jurassic "Tongue of the ocean" infilled with oolitic sands: the Belluno Trough, Venetian Alps, Italy. *Marine Geology*, 44: 59-95, Amsterdam.
- Bragin N. Yu., Tekin U.K. & Özçelik Y. (2002) - Middle Jurassic radiolarians from the Akgöl Formation, central Pontids, northern Turkey. *N. Jb. Geol. Paläont. Mb.*, 10: 609-628, Stuttgart.
- Buser S. (1986) - Osnovna geoloska karta SFRJ 1: 100 000 list Tolmin in Videm (Basic geological map of Yugoslavia 1: 100 000 sheet Tolmin and Videm). Zvezni geol. Zavod Beograd, Beograd.

- Buser S. (1987) - Tolmac k Osnovni geoloski karti SFRJ 1: 100 000 lista Tolmin in Videm (Explanatory text for Tolmin and Videm sheet). Zvezni geol. Zavod Beograd, 103 pp. Beograd.
- Buser S. (1989) - Development of the Dinaric and the Julian Carbonate Platforms and of the intermediate Slovenian Basins (NW Yugoslavia). *Mem. Soc. Geol. Ital.*, 40: 313-320, Roma.
- Buser S. (1996) - Geology of western Slovenia and its paleogeographic evolution. In: Drobne K., Goričan S. & Kotnik B. (eds.)- The role of Impact Processes in the Geological and Biological Evolution of Planet Earth. International workshop, ZRC SAZU: 111-123, Ljubljana.
- Buser S. & Debeljak I. (1996) - Lower Jurassic beds with bivalves in south Slovenia. *Geologija*, 37/38 (1994/95): 23-62, Ljubljana.
- Cattaneo A. & Steel R.J. (2003) - Transgressive deposits: a review of their variability. *Earth-Science Reviews*. 62: 187-228, Amsterdam.
- Channell J.E.T, D'Argenio B & Horváth F. (1979) - Adria, the African Promontory, in Mesozoic Mediterranean Palaeogeography. *Earth Science Reviews*, 15: 213-292, Amsterdam.
- Chiari M, Marcucci M. & Prella M. (2002) - New species of Jurassic radiolarians in the sedimentary cover of ophiolites in the Mirdita area, Albania. *Micropaleontology*, 48, supplement 1: 61-87, New York.
- Chiocchini M., Farinacci A., Mancinelli A., Molinari V. & Potetti M. (1994) - Biostratigrafia a foraminiferi, dasciudadali e calpionelle delle successioni carbonatiche dell' Appennino centrale (Italia). *Studi Geol. Camerti, Spec. Publ.*, 9-129, Camerino.
- Clari P. & Masetti D. (2002) - The Trento Ridge and the Belluno Basin. In: Santantonio M. (ed.)- General Field Trip Guidebook, VI International Symposium on the Jurassic System, 12-22 September 2002: 271-315, Palermo.
- Cobianchi M. & Picotti V. (2001) - Sedimentary and biological response to sea-level and palaeoceanographic changes of a Lower-Middle Jurassic Tethyan platform margin (Southern Alps, Italy). *Palaeogeogr., Palaeoclim., Palaeoecol.*, 169: 219-244, Amsterdam.
- Cousin M. (1970) - Esquisse géologique des confins italo-yougoslaves: leur place dans les Dinarides et les Alpes méridionales. *Bull. Soc. Géol. France*, 12: 1034-1047, Paris.
- Cousin M. (1981) - Les rapports Alpes-Dinarides. Les confins de l'Italie et de la Yougoslavie. *Soc. Géol. Nord*, Publ. No 5, Vol. 1 of 521 pp., Vol. 2 – Annexe of 521 pp., Villeneuve D'Ascq.
- Di Stefano P., Galacz A., Mallarino G., Mindszenty A. & Vörös A. (2002) - Birth and Early Evolution of a Jurassic Escarpment: Monte Kumeta, Western Sicily. *Facies*, 46: 273-298, Erlangen.
- Di Stefano P. & Mindszenty A. (2000) - Fe-Mn encrusted 'Kamenitza' and associated features in Jurassic of Monte Kumeta (Sicily): subaerial and/or submarine dissolution. *Sedim. Geology*, 132: 37-68, Amsterdam.
- Dogliani C. & Bosellini A. (1987) - Eoalpine and mesoalpine tectonics in the Southern Alps. *Geol. Rundsch.*, 76: 735-754, Stuttgart.
- Dogliani C. & Siorpaes C. (1990) - Polyphase deformation in the Col Bechei area (Dolomites-Northern Italy). *Eclogae geol. Helv.*, 83: 701-710, Basel.
- Dozet S. (1994) - Malmian bauxites at Kocevka reka and Kocevje. *RMZ-materials and geoenvironment*. 41: 215-219, Ljubljana
- Dozet S., Misić M. & Zuza T. (1996) - Malm Bauxite Occurrences in Logatec, Nanos and Kocevje are. *RMZ-materials and geoenvironment*, 43/1-2: 23-35, Ljubljana
- Dromart G., Allemand P., Garcia J-P & Robin C. (1996) - Variation cyclique de la production carbonatée au Jurassique le long d'un transect bourgonge-Ardèche, Est-France. *Bull. Soc. Géol. France*, 167/3: 423-433, Paris
- Dumitrica P., Immenhauser A. & Dumitrica-Jud R. (1997) - Mesozoic radiolarian biostratigraphy from Masirah Ophiolite, Sultanate of Oman. Part 1: Middle Triassic, uppermost Jurassic and Lower Cretaceous spumellarians and multisegmented nassellarians. *Bull. National Museum Natural Science*, 9: 1-106, Taichung.
- Elmi S. (1990) - Stages in the evolution of late Triassic and Jurassic carbonate platforms: the western margin of the Subalpine Basin (Ardèche, France). In: Tucker M. E., Wilson J.L., Crevello P.D., Sarg J.R. & Read S.F. (eds.)- Carbonate Platforms Facies, Sequences and Evolution. *Spec. Publ. Int. Ass. Sediment.*, 9: 109-144, Oxford.
- Emery D. & Myers K.J. (1996) - Sequence Stratigraphy. V. of 297 pp., Blackwell Science, Oxford.
- Goričan S. (1994) - Jurassic and Cretaceous radiolarian biostratigraphy and sedimentary evolution of the Budva Zone (Dinarides, Montenegro). *Mém. Géologie*, 18: 177 pp., Lausanne.
- Goričan S, Šmuc A. & Baumgartner P. (2003) - Toarcian Radiolaria from Mt. Mangart (Slovenian-Italian border) and their paleoecological implications. *Marine Micropaleontology*, 49: 275-301, Amsterdam.
- Graciansky P., Jacquin T. & Hesselbo S.P. (1998) - The Ligurian cycle: an overview of Lower Jurassic 2nd-order transgressive/regressive facies cycles in Western Europe. In: Graciansky, P., Hardenbol, J., Jacquin, T. & Vail, P.R. (eds.) - Mesozoic and Cenozoic Sequence Stratigraphy of European Basins, *SEPM Special Publications*, 60: 467-479, Tulsa.
- Grün B. & Blau J. (1997) - New aspects of calpionellid biochronology: proposal for revised calpionellid zonal and subzonal divisions. *Revue Paléobiol. Genève.*, 16/1: 197-214, Genève.
- Harris L.C. & Whiting B.M. (2000) - Sequence-stratigraphic significance of Miocene to Pliocene glauconite-rich layers, on- and offshore of the US Mid-Atlantic Margin. *Sedim. Geology*, 134: 129-147, Amsterdam
- Halamić J., Goričan S., Slovenec D. & Kolar-Jurkovek T. (1999) - A Middle Jurassic Radiolarite-Clastic Succession from the Medvednica Mt. (NW Croatia). *Geol. Croat.*, 52/1: 29-57, Zagreb.

- Hull D.M. (1997) - Upper Jurassic Tethyan and southern Boreal radiolarians from western North America. *Micropaleontology*, 43, supplement 2: 1-202, New York.
- Jacquin T. & Graciansky P. (1998) - Major transgressive/regressive cycles: the stratigraphic signature of European basin development. In: Graciansky P., Hardenbol J., Jacquin T. & Vail P.R. (eds.)- Mesozoic and Cenozoic sequence Stratigraphy of European Basins, *SEPM Special Publ.*, 60: 15-29, Tulsa.
- Jacquin T., Dardeau G., Durlet C., Graciansky P. & Hantzpergue P. (1998) - The North Sea Cycle: An Overview of 2nd-order Transgressive/Regressive Facies Cycles in Western Europe. In: Graciansky P., Hardenbol J., Jacquin T. & Vail P.R. (eds.)- Mesozoic and Cenozoic sequence Stratigraphy of European Basins, *SEPM Special Publication*, 60: 445-466, Tulsa.
- Jenkyns H.C. (1985) - The Early Toarcian and Cenomanian-Turonian anoxic events in Europe: comparison and contrasts. *Geol. Rundsch.*, 74/3: 505-518, Stuttgart.
- Jenkyns H.C. (1988) - The Early Toarcian (Jurassic) Anoxic Event: Stratigraphic, Sedimentary and Geochemical Evidence. *Am. J. Science*, 288: 101-151, New Haven.
- Jenkyns H.C. & Clayton C.J. (1986) - Black shales and carbon isotopes in pelagic sediments from the Tethyan Lower Jurassic. *Sedimentology*, 33: 87-106, Oxford.
- Jenkyns H.C., Sarti M., Masetti D. & Howarth M. K. (1985) - Ammonites and stratigraphy of Lower Jurassic black shales and pelagic limestones from the Belluno trough, Southern Alps, Italy. *Eclogae geol. Helv.*, 72/2: 299-311, Basel.
- Jenkyns H.C., Gèzy B. & Marshall J.D. (1991) - Jurassic manganese carbonates of Central Europe and the Early Toarcian Anoxic Event. *J. Geology*, 99/2: 137-149, Chicago.
- Jurkovsek B., Sribar L., Ogorelec B. & Jurkovsek T (1990) - Pelagic Jurassic and Cretaceous beds in the western part of the Julian Alps. *Geologija*, 31/32 (1988/1989): 285-328, Ljubljana.
- Kiessling W. (1996) - Facies Characterisation of Mid-Mesozoic Deep-Water Sediments by Quantitative Analysis of Siliceous Microfaunas. *Facies*, 35: 237-274, Erlangen.
- Kocher R.N. (1981) - Biochronostratigraphische Untersuchungen oberjurassischer radiolarienführender Gesteine, insbesondere der Südalpen. *Mitt. Geol. Ins. ETH u. Univ. Zürich*, N. F., 234: 1-184, Zürich.
- Kozur H. (1984) - New radiolarian taxa from the Triassic and Jurassic. *Geol. Paläont. Mitt. Innsbruck*, 13/2: 49-88, Innsbruck.
- Kozur H. (1991) - The evolution of the Meliata-Hallstatt ocean and its significance for the early evolution of the Eastern Alps and Western Carpathians. *Palaeogeogr., Palaeoclim., Palaeoecol.*, 87: 109-135, Amsterdam.
- Mallarino G., R.H. Goldstein & Di Stefano P. (2002) - New approach for quantifying water depth applied to the enigma of drowning of carbonate platforms. *Geology*, 30/9: 783-786, Tulsa.
- Martire L. (1992) - Sequence stratigraphy and condensed pelagic sediments. An example from the Rosso Ammonitico Veronese, northeastern Italy. *Palaeogeogr., Palaeoclim., Palaeoecol.*, 94: 169-191, Amsterdam.
- Martire L. (1996) - Stratigraphy, Facies and Synsedimentary Tectonics in the Jurassic Rosso Ammonitico Veronese (Altopiano di Asiago, NE Italy). *Facies*, 35: 209-236, Erlangen.
- Masetti D. & Bianchin G. (1987) - Geologia del gruppo della Schiara (Dolomiti Bellunesi). *Mem. Scien. Geol.* 39: 187-212. Padova.
- Mattioli E. & Pittet B. (2002) - Contribution of calcareous nannoplankton to carbonate deposition: a new approach applied to the Lower Jurassic of central Italy. *Marine Micropaleontology*, 45:175-190, Amsterdam.
- Morettini E., Santantonio M., Bartolini A., Cecca F., Baumgartner P.O. & Hunziker J.C. (2002) - Carbon isotope stratigraphy and carbonate production during the Early-Middle Jurassic: examples from the Umbria-Marche-Sabina Apennines (central Italy). *Palaeogeogr., Palaeoclim., Palaeoecol.*, 184/3-4: 251-273, Amsterdam.
- Mutti E. (1992) - Turbidite Sandstones. V. of 275 pp. Agip, Milano.
- Odin G.S. & Fullagar P.D. (1988) - Geological significance of the glaucony facies. In: Odin, G.S. (ed.) - Green Marine Clays: 295-332, Amsterdam.
- Piper D.J.W. & Stow D.A.V. (1991) - Fine-Grained Turbidites. In: Einsele G., Ricken W. & Seilacher A.(eds.)- Cycles and Events in Stratigraphy: 360-376, Berlin, Springer Verl.
- Pittet B. & Mattioli E. (2002) - The carbonate signal and calcareous nannofossil distribution in an Upper Jurassic section (Balingen-Tieringen, Late Oxfordian, southern Germany). *Palaeogeogr., Palaeoclim., Palaeoecol.*, 179: 71-96, Amsterdam.
- Placer L. (1999) - Contribution to the macrotectonic subdivision of the border region between Southern Alps and External Dinarides. *Geologija*, 41 (1998): 223-255, Ljubljana.
- Placer L. & Car J. (1998) - Structure of Mt. Blegos between the Inner and Outer Dinarides. *Geologija*, 40: 305-323, Ljubljana.
- Prela M., Chiari M. & Marcucci M. (2000) - Jurassic radiolarian biostratigraphy of the sedimentary cover of ophiolites in the Mirdita area, Albania: new data. *Ofioliti*, 25/1: 55-62, Firenze.
- Remane J. (1985) - Calpionellids. In: Bolle H.M., Saunders J.B. & Perch-Nielsen K. (eds.)- Plankton Stratigraphy. *Cambridge Univ. Press*: 555-572, Cambridge.
- Rozic B. (2003a) - Sedimentološke raziskave srednje in zgornjejurskih kamnin Slovenskega jarka v profilu Zaposkar. *Geoloski zbornik-povzetki referatov*, 17: 146-149. Ljubljana.
- Rozic B. (2003b) - Basin margin evolution: Middle and Upper Jurassic succession of Slovenian Basin. In: Velic I. (ed.)- Abstract book of 22nd Meeting of Sedimentology -Opatija 2003: 180, Opatija.
- Santantonio M. (1994) - Pelagic Carbonate Platforms in the Geologic Record: Their Classification, and Sedimen-

- tary and Paleotectonic Evolution. *AAPG Bulletin*, 78/1: 122-141, Tulsa.
- Santantonio M. & Muraro C. (2002) - The Sabina Plateau, Palaeoescarpment, and Basin – Central Apennines. In: Santantonio M. (ed.)- General Field Trip Guidebook on VI International Symposium on the Jurassic System, 12-22 September 2002: 271-315, Palermo.
- Sashida K., Munasri S., Adachi S. & Kamata Y. (1999) - Middle Jurassic radiolarian fauna from Rotti Island, Indonesia. *J. Asian Earth Sciences*, 17: 561-572, Amsterdam.
- Schlager W., Reijmer J.J.G. & Droxler A. (1994) - Highstand shedding of carbonate platforms. *J. Sedim. Research*, B64/3: 270-281, Tulsa.
- Sykora M. & Ozvoldova L. (1996) - Lithoclasts of Middle Jurassic radiolarites in debris flow sediments from Silica Nappe (locality Bleskovy pramen, Slovak Karst, Western Carpathians). *Mineralia Slovaca*, 28: 21-25, Bratislava.
- Weissert H.J. (1979) - Die Palaeoozeanographie der sudwestlichen Tethys in der Unterkreide. *Mitt. Geol. Inst. ETH u. Univ. Zürich*, N.F., 226: 174 pp., Zürich.
- Weissert H. & Mohr H. (1996) - Late Jurassic climate and its impact on carbon cycling. *Palaeogeogr., Palaeoclim., Palaeoecol.*, 122: 27-43, Amsterdam.
- Widz D. & De Wever P. (1993) - Nouveau nassellaires (Radiolaria) des radiolarites jurassiques de la coupe de Szeligowy Potok (Zones de Klippes de Pieniny, Carpathes occidentales, Pologne). *Rev. de Micropal.*, 36/1: 77-91, Paris.
- Winterer E.L. (1998) - Paleobathymetry of Mediterranean Tethyan Jurassic pelagic sediments. *Mem. Soc. Geol. It.*, 53: 97-131, Roma.
- Winterer E.L. & Bosellini A. (1981) - Subsidence and sedimentation on Jurassic passive continental margin, Southern Alps, Italy. *AAPG Bulletin*, 65: 394-421, Tulsa.
- Wright V.P. & Burchette T.P. (1996) - Shallow-water carbonate environments. In: Reading H.G. (ed.) – Sedimentary Environments: Processes, Facies and Stratigraphy: 325-394, Blackwell Science, Oxford.
- Yang Q. & Wang Y. (1990) - A taxonomic study of Upper Jurassic Radiolaria from Rutog County, Xizang (Tibet). *Acta Micropalaeontologica Sinica*, 7/3: 195-218, Beijing.
- Zempolich W.G. (1993) - The drowning succession in Jurassic carbonates of the Venetian Alps, Italy: a record of supercontinent breakup, gradual eustatic rise and eutrophication of shallow water environments. In: Louks R.G. & Sarg J.F. (eds.) - Carbonate sequence stratigraphy. *Amer. Ass. Petr. Geol. Mem.*, 57: 63-105, Tulsa.
- Zempolich W.G. & Erba E. (1999) - Sedimentologic and chemostratigraphic recognition of third-order sequences in resedimented carbonate: the Middle Jurassic Vajont Limestone, Venetian Alps, Italy. In: Harris P.M., Saller A.H. & Simo J.A. (eds.) – Advances in Carbonate Sequence Stratigraphy: Application to Reservoirs, Outcrops and Models. *SEPM Special Publication*, 63: 335-370, Tulsa.
- Zügel P., Riegraf W., Schweigert G. & Dietl G. (1998) - Radiolaria from the Nusplingen Lithographic Limestone (Late Kimmeridgian, SW Germany). *Stuttgarter Beitr. Naturk.*, Ser. B 268: 1-43, Stuttgart.